Deformation and uplift at the transition from oceanic to continental subduction, Sumba Island, Indonesia

Christine Authemayou, Kevin Pedoja, Denovan Chauveau, Laurent Husson, Gilles Brocard, Bernard Delcaillau, Julie Perrot, Sonny Aribowo, Sri Yudawati Cahyarini, Mary Elliot, et al.

Journal of Asian Earth Sciences
September 2022, Volume 236, Pages 105316 (15p.)
https://doi.org/10.1016/j.jseaes.2022.105316
https://archimer.ifremer.fr/doc/00780/89196/

Deformation and uplift at the transition from oceanic to continental subduction, Sumba Island, Indonesia

Authemayou Christine [1,*], Pedoja Kevin [2], Chauveau Denovan [1], Husson Laurent [3], Brocard Gilles [4], Delcaillau Bernard [2], Perrot Julie [1], Aribowo Sonny [3,5], Yudawati Cahyarini Sri [5], Elliot Mary [6], Hilman Natawidjaja Danny [5], Scholz Denis [7]

[1] Univ Brest, CNRS, Ifremer, Geo-ocean, UMR6538, F-29850 Plouzané, France
[2] M2C UMR 6143, Université de Caen-Normandie, France
[3] ISTerre, CNRS, UMR 5275, Université de Grenoble Alpes, Grenoble, France
[4] Archéorient, UMR 5133, MOM, Université de Lyon 2, Lyon, France
[5] Research Center for Geotechnology, Indonesian Institute of Sciences, LIPI, Bandung, Indonesia LPG
[6] CNRS, UMR 6112, Université de Nantes, Nantes, France
[7] Institute for Geosciences, University of Mainz, Mainz, Germany

* Corresponding author : Christine Authemayou, email address : christine.authemayou@univ-brest.fr

Abstract :

The transition along the strike of the Sunda subduction zone, from oceanic subduction in the west to subduction of continental Australian lithosphere in the east is envisioned as one of the canonical examples of the structural changes that take place within an overriding plate when a continental lithosphere wedge enters a subduction zone. Yet, the along-strike offset of the trench toward the Australian margin represents a structural response opposite to the predictions of numerical models. To understand this paradox, we analyse the morphotectonic evolution of Sumba island located at the transition from oceanic to continental Indo-Australian lithosphere subduction. Drainage evolution allows us to constrain the topographic evolution of the island since the Pliocene. Flights of uplifted coral reef terraces document Quaternary deformation. Focal mechanisms of shallow crustal earthquakes constrain the current stress field. Together, these data reveal that the island is affected by dextral en-échelon folding. Offshore, west of the island, reverse and strike-slip focal mechanisms evidence an active dextral transpressional zone. The emergence of the island and dextral shearing of the accretionary prism were triggered by subduction of the western lateral boundary of the Australian continental margin. We contend that the Plio-Quaternary tectonic evolution of the region, with transpression and migration of the trench toward the Australian margin is primarily dictated by shear stress transfer from the lower plate to the overriding plate, favored by strong interplate coupling, and by southwestward escape of the Savu-Sumba block following the impingement of the Australian continental margin against Timor island.

Highlights

► The Australian margin boundary collision produces forearc dextral transpression. ► Interplate transfer of shear stress and forearc block escape induce trench migration. ► Northeastward folding has been propagating across Sumba Island since the Pliocene. ► One-third of Sumba Island was inundated by flexure and gravitational collapse.

Keywords : Sumba, tectonics, drainage reorganization, coral reef terrace sequences, transition oceanic subduction/ continental subduction

1. Introduction

The entrance of a continental lithospheric wedge into a subduction zone, where oceanic lithosphere was previously subducted, generates marked structural changes in the forearc region of the overriding plate. Numerical and analogue models (Royden and Husson, 2009; Boutelier et al., 2012; Guillaume et al., 2013; Magni et al., 2014; Moresi et al., 2014) suggest that subduction stalls in front of the buoyant downgoing continental margin, while the subduction of surrounding oceanic slabs continues unabated. The roll-back of these oceanic slabs relative to the stalled continental margin progressively offsets the trench across the transition between the oceanic and continental lithospheres (Harris, 1992). This offset accommodates most of the gradient in subduction rates that result from the slowing down of subduction in front of the continental lithosphere. Additionally, this offset allows the extrusion of the overriding plate away from the colliding continental margin, toward surrounding oceanic subduction zones. These models also predict lateral bending of the downgoing slab where the plate boundary is offset, which may ultimately lead to the tearing of the downgoing slab (Guillaume et al., 2013; Magni et al., 2014).

The along-strike transition from oceanic subduction to incipient continental collision along Sunda-Banda arc is one of few such transitions currently occurring on Earth (Fig. 1). However, over geological time, such geodynamic arrangements occur frequently. Much knowledge is to be gained, therefore, from the study of modern examples. In the case at hand, no lateral offset of the trench toward the oceanic domain is observed at the transition between oceanic subduction and incipient continental collision. The extent of the continental and oceanic domains in the down going slab remains controversial, and the seismic imaging

of the slab does not resolve the details of slab deformation across the transition zone (Widiyantoro and van der Hilst, 1996; Hall and Spakman, 2015; Zenonos et al., 2019; Harris et al., 2020). Within the overriding plate, the ocean-continent transition is marked by a rapid enlargement of the accretionary prism in the southwestern part of the Savu basin, below the southern part of Sumba ridge (Harris, 1991; Rigg and Hall, 2011, Fig. 1). The lack of slab retreat toward the oceanic domain, together with the absence of an obvious slab tear (Harris et al., 2020), may attest of the youth of the subduction of the continental margin. In the meantime, however, the structure of the accretion prism and the activity of the back-arc Wetar thrust (Baillie et al., 2019) suggests that the subduction of the Australian continent has already significantly deformed the overriding Sunda arc.

We investigate the morphotectonic evolution of Sumba Island in order to better document the changes associated with the under-thrusting of the Australian continental wedge below the Sunda-Banda arc. Sumba Island is conveniently located in the fore-arc of the Sunda-Banda arc within the transition zone, behind the area of widening of the accretionary prism (Fig. 1). The island emerged during Pliocene times and has kept uplifting ever since (Fortuin, 1997, Fleury et al., 2009; Nexer et al., 2015). We conducted a tectonic and geomorphological analysis of the island by measuring structural markers of deformation, and by analyzing the deformation of Holocene to Pleistocene coral reefs fringing the western, northern, eastern and, for the first time, southern coasts of the island. Deformation at higher elevation, and over longer time scales is assessed using the evolution of Pliocene and younger river networks. We use these data to reconstruct the pattern of uplift during different time intervals. We then integrate these results within the current regional tectonic stress field, inferred from shallow earthquake focal mechanisms. We finally discuss the contribution of interplate coupling to the evolution of upper plate deformation and trench migration over time, and propose a tectonic evolution involving lateral changes in crustal

thickness in the downgoing and overriding plates, as well as lateral motions of upper plate forearc basement blocks.

2. Geological setting

Within the Indonesian Archipelago, the 80 km wide, 200 km long Sumba Island is located in the Sunda-Banda fore-arc, north of the transition from oceanic to continental subduction (Fig. 1). West of Sumba, the Indian-Australian oceanic plate subducts northward at 80 $mm \cdot yr^{-1}$ (relative to a fixed Sunda shelf reference frame) beneath the Sundaland part of the Eurasian plate along the Java trench, with weak interplate coupling (Pacheco et al., 1993; Simons et al., 2007, Nugroho et al., 2009; Hall et al., 2011). East of Sumba, the rifted passive margin of the Australian continental lithosphere is overridden by the Banda arc at 21 $mm \cdot yr^{-1}$ along the Timor trench, beneath the Banda oceanic domain, with strong interplate coupling (Bock et al., 2003; Nugroho et al., 2009, Fig. 1). South of Sumba Island, the plate boundary is offset 150 km-long to the south, linking the Java trench and Timor trough. Termination of oceanic subduction along the Java trench and transition to arc-continent collision along the Timor trough has triggered transcurrent reactivation of NE-SW-trending mesozoic syn-rift structures of the Australian passive margin (Hengesh and Whitney, 2016; Fig. 1A). Within the overriding plate, the transition zone coincides with Sumba Ridge, an isolated rigid block between the trench and the active volcanic arc, embedded within more deformable accreted sediments of the prism (Fig. 1B). It is interpreted as the basement of a volcanic arc that formed during Late Cretaceous-Paleocene time, south of the Sundaland block (Rangin et al., 1990; Wensink and Bergen, 1995; Rutherford et al., 2001; Hall, 2012; Hall and Smyth, 2008; Satyana and Purwaningsih, 2011). Sediments above this basement have been

interpreted as autochtonous sediments deposited in the Late Cretaceous-Paleocene at the back of the accretionary prism (Fortuin et al, 1992, 1997; Abdullah et al., 2000; Fleury et al., 2009; Satyana and Purwaningsih, 2011). The inner and younger Banda volcanic arc has formed northeast of Sumba Island over the past 15 Ma, as a result of the subduction of a Jurassic oceanic basin, bounded by continental crust, within the Australian plate (Hamilton, 1979; Spakman and Hall, 2010).

Sumba Ridge marks the transition from the western Lombok fore-arc basin to the eastern Savu fore-arc basin (Hamilton, 1979; Rutherford et al., 2001; Hall and Smyth, 2008; Harris et al., 2009; Harris, 2011). The Lombok basin is underlain either by 9 to 11 km-thick oceanic crust, formed during the Cretaceous to middle Eocene opening of the Indian Ocean (Planert et al., 2010), or by thinned rifted continental crust, transitioning eastward into a crust of mixed continental/oceanic composition (Lüschen et al., 2011), and overlain by > 4-5 km of tertiary sediments (Planert et al., 2010; Kopp, 2011; Lüschen et al., 2011). Below the Sumba Ridge and the Savu Basin (Fig. 1B), the upper plate Moho lies at depths of ~26-27 km (Shulgin et al., 2009). The floor of the Savu Basin was close to sea level in the Early Miocene, but subsequently underwent extension and rapid subsidence during the Middle Miocene (Shulgin et al., 2009; Spakman and Hall, 2010; Rigg and Hall, 2011). On Sumba Island, this extensional event generated down-to-the-east normal faults, major subsidence in the eastern part of the island, mega-slumps, turbidites and intra-formational fault scarps (Von Der Borch et al., 1983; VanderWerff et al., 1994; Fortuin et al., 1994; 1997). The eastward deepening of depositional environments is indicated by shallow-water carbonate platform deposits (Waikabubak formation), which are restricted to the western part of the island and pelagic sediments (Kannanggar formation) deposited at depths of ~5000 m in the east. During the Late Miocene and Early Pliocene, the arrival of the Australian continent into the trench shortened and uplifted the fore-arc domain (e.g., Harris, 1991; Fortuin et al., 1997;

Hall and Smyth, 2008; Haig 2012; Tate et al., 2017; Miller et al., 2021). Its earliest manifestation, offshore eastern Sumba, is a northward tilting of the Tortonian sediments of the Kannanggar formation (Fortuin et al., 1992; 1997; Fig. 2). Emergence of the eastern part of the Sumba Island occurred around 3 Ma ago (Roep and Fortuin, 1996). Deformation then propagated southeastward (Rigg and Hall, 2011), leading to the emergence of Savu island at 1.9 Ma (Harris et al., 2009), and then of Rote island since 0.2 Ma (Roosmawati and Harris, 2009). Continued uplift on Sumba Island during the Quaternary is recorded by the emergence of coral reef terrace sequences (e.g., Pirazzoli et al., 1991; 1993; Bard et al., 1996, Fig. 2). Fleury et al. (2009) noticed that the sequences are tilted to the north and are affected by gravitational collapse in the south. They consider that tilting and collapse resulted from the subduction of a seamount beneath Sumba. Miller et al. (2021) used ambient noise tomography and geochemistry of the volcanic arc to conclude that the rapid uplift of Sumba is related to the subduction of a volcanic ridge, ahead of the Australian continental crust. Gravitational collapse has generated normal faults along the southern flank of the island. Faulting has progressively expanded northward, and now also affects the northern side of the island (Fig. 2). Authemayou et al. (2018) proposed that the western part of Sumba is a broad asymmetric E-W anticline, and that the northward tilting of the coral reef terraces occurs along the shallow-dipping northern limb of this anticline.

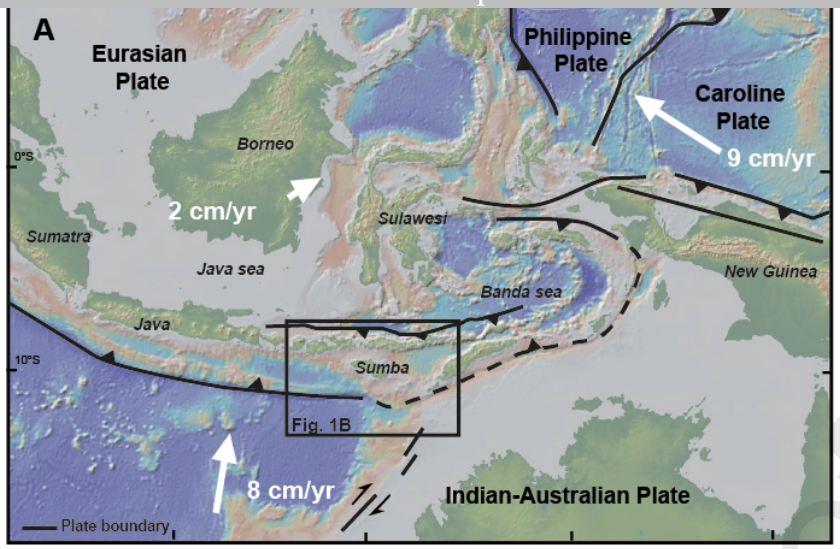
A
Eurasian Plate
Philippine Plate
Caroline Plate
9 cm/yr
Borneo
2 cm/yr
Sulawesi
Sumatra
Java sea
New Guinea
Banda sea
Java
Sumba
Fig. 1B
8 cm/yr
Indian-Australian Plate
Plate boundary

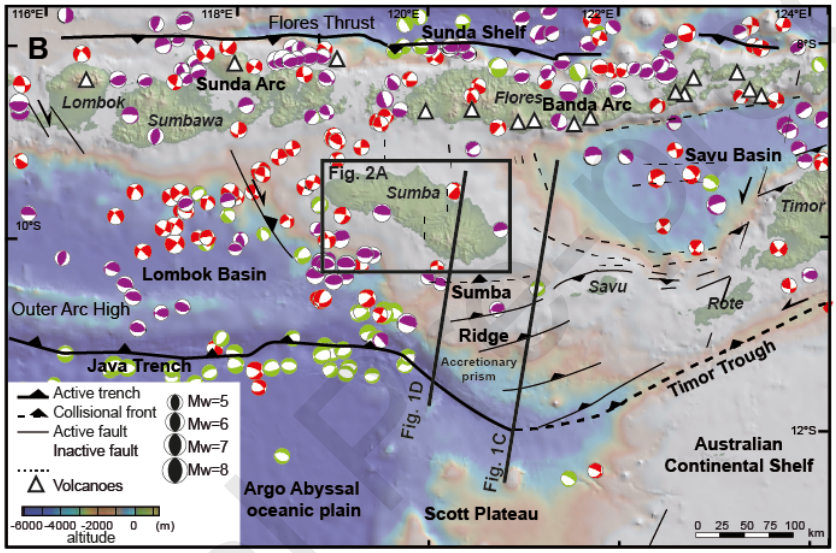
B
Flores Thrust
Sunda Shelf
Sunda Arc
Lombok
Sumbawa
Flores
Banda Arc
Savu Basin
Fig. 2A
Sumba
Timor
Lombok Basin
Outer Arc High
Sumba Ridge
Savu
Rote
Java Trench
Accretionary prism
Timor Trough
Fig. 1D
Fig. 1C
Australian Continental Shelf
Argo Abyssal oceanic plain
Scott Plateau
Active trench
Collisional front
Active fault
Inactive fault
Volcanoes
Mw=5
Mw=6
Mw=7
Mw=8
altitude

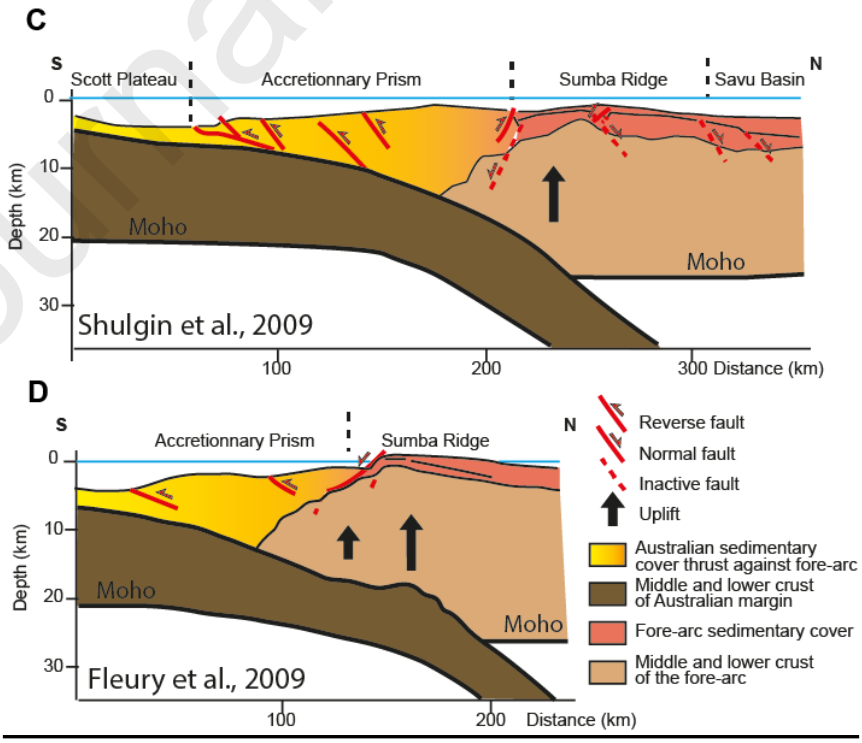
C
S
N
Scott Plateau
Accretionnary Prism
Sumba Ridge
Savu Basin
Depth (km)
Moho
Moho
Shulgin et al., 2009
Distance (km)
D
Accretionnary Prism
Sumba Ridge
Moho
Moho
Fleury et al., 2009
Distance (km)
Reverse fault
Normal fault
Inactive fault
Uplift
Australian sedimentary cover thrust against fore-arc
Middle and lower crust of Australian margin
Fore-arc sedimentary cover
Middle and lower crust of the fore-arc

Figure 1: Geodynamic settings of Indonesia (A) and of Sumba Island (B), modified from Rigg and Hall (2011; 2012) and Lűschen et al (2011). Focal mechanisms of shallow earthquakes (<50km) from GCMT solutions (http://globalcmt.org; **Dziewonski et al., 1981; Ekström et al., 2012). Colors indicate focal mechanism types (green: normal faulting, red: strike-slip faulting, purple: reverse faulting). C) NS-striking section across the Sumba Ridge, east of Sumba Island, modified from Shulgin et al. (2009). (D) NS-striking geological section across Sumba Island, modified from Fleury et al. (2009).**

3. Methods

3.1. Morphological identification of land surface deformation

We mapped fault traces on Sumba Island based on drainage analysis and their geomorphic expression using the 12 m-resolution TanDEM-X Digital Elevation Model, and the 10.5 m- to 1.5 m-resolution Pleiades and 6-7 SPOT satellite images, provided by the CNES (i.e. Centre National d'Études Spatiales). The mapping of remote sensing data was ground-checked in 2017 and included collecting measurements of the orientation of Miocene beds (Fig. 2).

A detailed review of the geomorphic evolution and the processes driving river rearrangement of western Sumba is provided in Authemayou et al. (2018). The analysis is here extended to the central and the eastern parts of Sumba (Figs. 3, 4). The theoretical map of the drainage network was extracted from the 12 m resolution TanDEM-X Digital Elevation Model using standard overland water routing procedures that involve the filling of closed topographic depressions. However, because karstic water routing is substantial on

some parts of the island, a visual rectification of the drainage lines was conducted using the optical satellite images (Pleiades and SPOT 6-7 satellite images). The comparison of predicted overland water routing and actual water routing helped us to assess the extent of endokarstic river networks (Authemayou et al., 2018). Stream segments of the surficial drainage were then classified according to their flow azimuth. The drainage network displays abundant river rerouting and flow reversal. To document river rerouting, we inventoried wind gaps left after rerouting events. To identify flow reversal, we inventoried fish hooks in the course of river tributaries close to their junctions with reversed trunk streams (Middleton et al. 1995). Windgaps consist of low-elevation, often flat-floored notches incised across ridges that separate conterminous river catchments. The windgaps have a distinctive morphology that allow them to be distinguished from common passes produced by the simple lowering of ridge crests by slope erosion. Their steep, ridge-transverse flanks stand in sharp contrast to the very shallow, ridge-transverse gradient of their floor. Such shallow gradient can only be achieved by bedrock erosion and sediment dispersal by fluvial processes, transverse to the ridges. The former flow direction through these windgaps relies on the identification of flow reversal in one of the two catchments now separated by the windgap. In the area of interest, flow reversal is evidenced by hooked tributaries present in the drainage of one of the two rivers that used to be connected through the windap. The current flow direction along the hooked tributaries is opposite to that of the trunk river, and represents the former direction of flow along the trunk river, toward the windgap.

3.2. Morphological delineation and correlation of uplifted reef terraces

Coral reef terraces were mapped to determine the recent deformation pattern of the island. The terraces are formed by different reefal limestone units constructed and eroded during successive Quaternary sea-level highstands (Chauveau et al., 2021). Maximum and

minimum elevations were extracted from the 12m-resolution TanDEM X elevation model along topographic swath profiles perpendicular and parallel to the long axis of Sumba Island. The TanDEM X elevation model was loaded into ESRI's ArcGIS 10 software and used to map the inner edge or back-edge, of the terraces using hillshade, contour, and slope maps and were validated in the field. The location of the inner edge was then refined using satellite images from Google. Particular care was given to the delineation of the terrace flights along the northern coast, which represent the most lateraly extensive and continuous geomorphological markers of deformation.

Efforts were focused on the terrace level represented by a thick black line on Figure 5, which was initially mapped along the whole northern coast of Sumba Island and correlated to MIS 11 (400 ± 20 ka) by Nexer et al. (2015). This terrace lies at an elevation of 190 ± 10 m at Cape Laundi (Pirazzoli et al., 1993). Lateral correlation of reef terraces across valleys, is based on the continuity of elevations, planform width, and equivalent position in the terrace sequence. A correlation of terraces based on these sole geomorphic criteria across the Kambaniru River valley (fig. 3) cannot be established with certainty, however, the continuity and expression of the MIS 11 terrace suggests it extends around the island. The morphological mapping was finally refined through direct observation in the field. At one site on the southern coast, a topographic survey of the coral reef terraces sequence was conducted using a real-time kinematic differential global positioning system (RTK DGPS).

The reef terraces were then projected onto the swath profiles, in order to document Quaternary uplift patterns. The different reef terraces were identified starting at Cape Laundi, where the chronostratigraphy of the terraces is well established (Pirazzoli et al., 1991; Pirazzoli et al., 1993; Bard et al.,1996), and from there were extended laterally throughout the entire coastal stretch (~350 km, Nexer et al., 2015). Tilting and folding of the terrace levels was analyzed by projecting the elevation of terrace inner edges along various strikes,

until the steepest dip angle was found (thus minimizing projection artefacts). Tilted coral reef terraces plot as straight lines on stacked-swath projections. Folded terraces display their maximal flexure when profiles are perpendicular to the fold axis.

3.3. Dating of uplifted coral reef terraces

At the site where the DGPS survey was undertaken, we sampled the lowest coral terrace for radiogenic ^{14}C and U/Th dating. A gastropod (sample SUM 18-12) was dated using ^{14}C accelerator mass spectrometry (Orsay, GEOPS). The gastropod shell was also dated using U/Th dating. Its calcite and aragonite contents were obtained using a XRD Brucker D8 at the LCG (Laboratoire d'étude des "Cycles Géochimiques et Ressources", IFREMER) in Brest (France). U/Th isotopic analysis was performed by multi-collector inductively coupled plasma mass spectrometry (MC-ICPMS) at the Institute for Geoscience, University of Mainz, Germany. For a detailed description of the methodology, the reader is referred to Obert et al. (2016), Yang et al. (2015) and Gibert et al. (2016).

3.4. Distribution of instrumental earthquakes

Focal mechanism solutions for earthquakes (Mw>5) were extracted from the Global Centroid Moment Tensor catalog for the period from 1976 to 2019 (GCMT, Dziewonski et al., 1981; Ekström et al., 2012, www.globalcmt.org) and were superposed on our structural and bathymetric maps (Fig. 1). A cut-off depth of 50 km depth was chosen to eliminate most earthquakes produced at the subduction interface and in the downgoing plate, in the fore-arc region. Nodal planes were interpreted as fault planes when their direction corresponded to the direction of a major bathymetric lineament located in their vicinity and/or when their direction corresponded to an alignment of focal mechanisms.

4. Results

4.1. Structural mapping

Miocene beds dip at shallow angles (<8° to 12°) on the northern and southern sides of the island. They are gently dipping (<4°) to flat-lying along the median axis of the island (Fig. 2). Strata dip conforms to the topography: Miocene beds are inclined towards the north along the northern side of the island, and towards the south along the southern side of the island, defining a broad E-W-trending anticlinal flexure. This flexure is best expressed in the westernmost and easternmost parts of Sumba. Two anticlines are mapped along the south coast of the island and are referred to as the eastern and western anticlines (Fig. 2). In the central region, however, the structural organization is more complex. Along the southern coast, in Keradu Bay and Tarimbang Bay, Miocene strata are tilted southeastward (5°), but 10 km to the south these deposits dip 9° to the northeast, revealing the nose of a tight syncline between the western and eastern anticlines (Fig. 2).

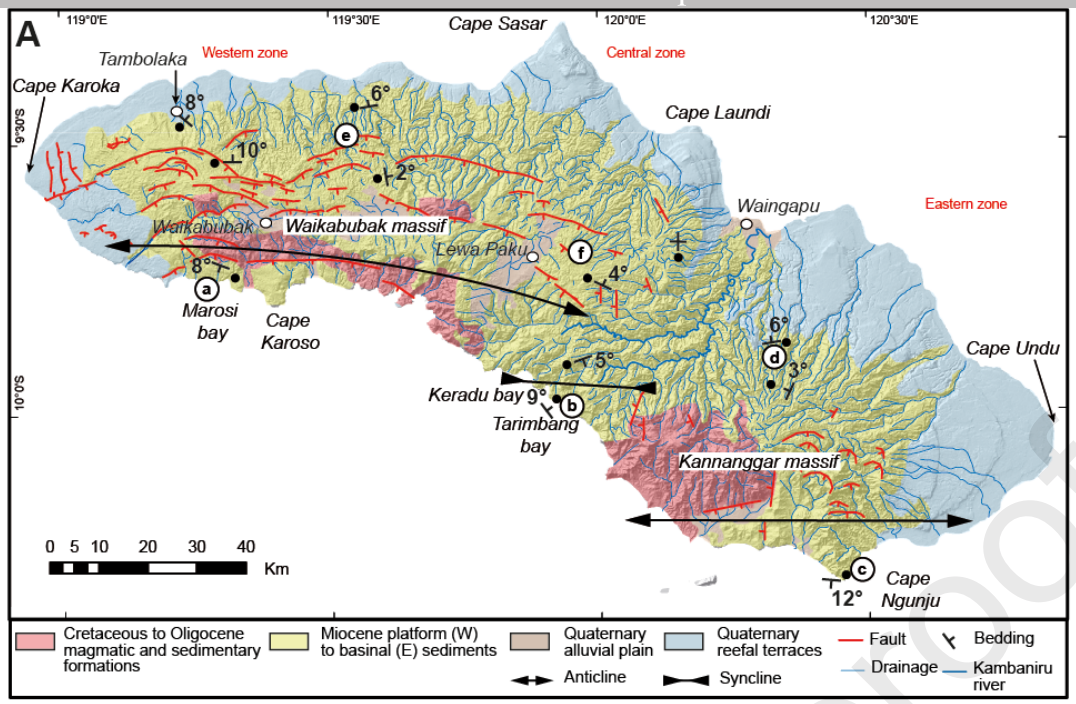
A
119°0'E
119°30'E
120°0'E
120°30'E
9°30'S
10°0'S
Cape Sasar
Western zone
Central zone
Eastern zone
Tambolaka
Cape Karoka
Cape Laundi
Waingapu
Waikabubak
Waikabubak massif
Lewa Paku
Marosi bay
Cape Karoso
Keradu bay
Tarimbang bay
Kannanggar massif
Cape Undu
Cape Ngunju
8°
6°
10°
2°
8°
4°
6°
3°
5°
9°
12°
a
b
c
d
e
f
0 5 10 20 30 40
Km
Cretaceous to Oligocene magmatic and sedimentary formations
Miocene platform (W) to basinal (E) sediments
Quaternary alluvial plain
Quaternary reefal terraces
Fault
Bedding
Drainage
Kambaniru river
Anticline
Syncline

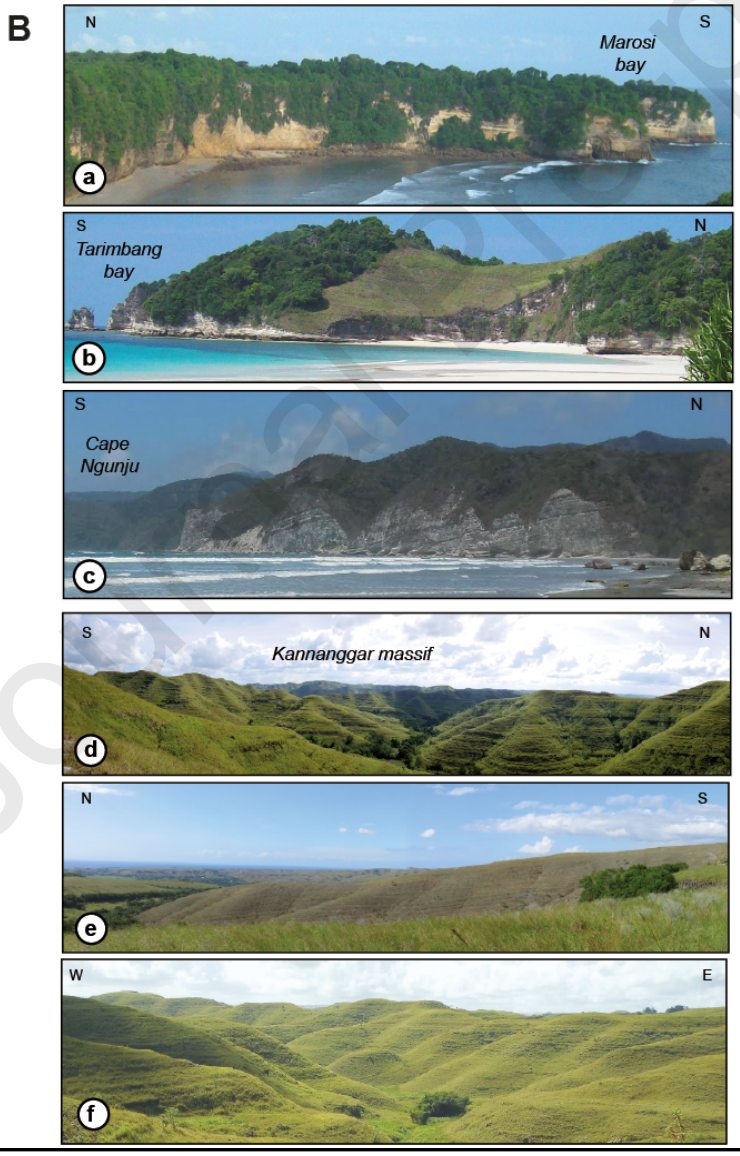
B
N
S
Marosi bay
a
S
N
Tarimbang bay
b
S
N
Cape Ngunju
c
S
N
Kannanggar massif
d
N
S
e
W
E
f

Figure 2: Geology and tectonics of Sumba island. (A) Shaded relief with main geological units, faults, and drainage lines. Fold axes are deduced from the structural measurments. (B) Photographs illustrating spatial variations in the dip of Miocene formations throughout the island (a, c, b, d, e, f). See Fig. 2A for location.

The faults manifest themselves as long lineaments that disrupt the topography and that do not coincide with lithological changes. Fault scarps were identified as sharp slope breaks that offset planar surfaces and streams. Differential uplift across the fault scarps has resulted in a change in fluvial dynamics across the upslope-facing fault scarps (Authemayou et al., 2018). We divided the distribution of normal faults into three zones (Western, Central and Eastern Sumba, Fig. 2A), based on changes in fault trace shape and fault array arrangements (Authemayou et al., 2018). In Western Sumba, the normal faults that disrupt the Waikabubak Plateau and the southern slope of the island are cuspate, imbricate, and have a down to the south sense of displacement (Fig. 2). In Central Sumba, the density of down to the south faults decreases, and NW-SE- to N-S-trending, short, down to the west normal faults are observed. In Eastern Sumba, a cluster of short, cuspate, down-to-the-south normal faults affect the top of the eastern part of the Kannanggar massif.

4.2. Drainage pattern

The main drainage divide of the island lies closer to the south coast than the north coast except at its western end (Fig. 3). While most streams flow away from the divide, some streams on the Waikabubak Plateau and around the Keradu Bay initially flow toward the divide before being captured by west-flowing, southwest-flowing or south-flowing streams

(Figs. 3 and 4). In some cases, the changes in flow directions are so large that they have the appearance of typical fish-hook tributaries (Fig. 3). The largest concentration of fish-hook tributaries is found near Keradu Bay between east-flowing and north-west-flowing streams (Fig. 4).

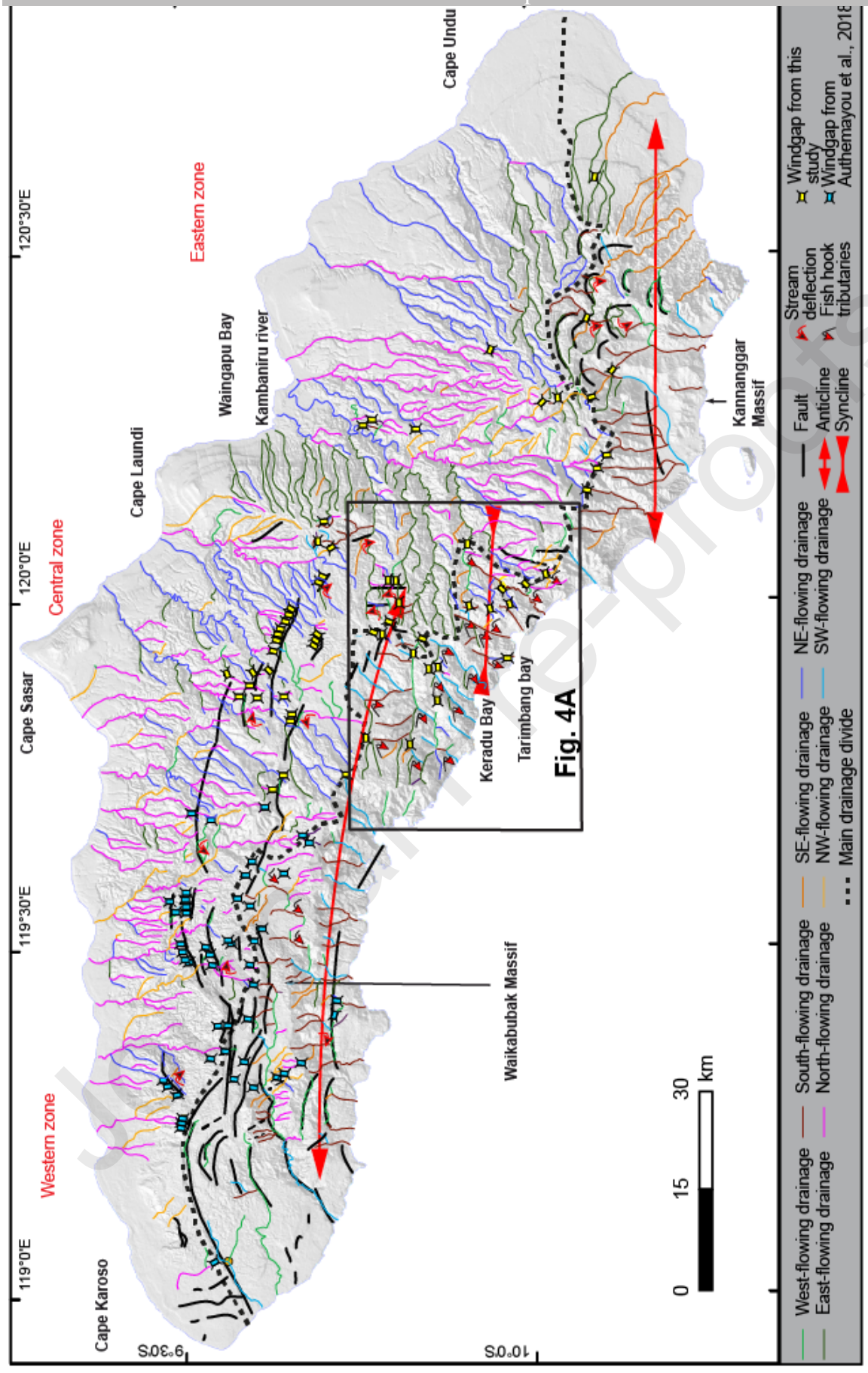
Cape Undu
Eastern zone
Waingapu Bay
Kambaniru river
120°30'E
Cape Laundi
Central zone
120°0'E
Cape Sasar
119°30'E
Western zone
119°0'E
Cape Karoso
9°30'S
10°0'S
Kannanggar Massif
Keradu Bay
Tarimbang bay
Fig. 4A
Waikabubak Massif
0
15
30
km
West-flowing drainage
East-flowing drainage
South-flowing drainage
North-flowing drainage
SE-flowing drainage
NW-flowing drainage
NE-flowing drainage
SW-flowing drainage
Main drainage divide
Fault
Anticline
Syncline
Stream deflection
Fish hook tributaries
Windgap from this study
Windgap from Authemayou et al., 2018

Figure 3: Geomorphologic map of the drainage pattern and tectonics features.

In the western and central parts of Sumba, numerous windgaps breach the normal fault scarps (Fig. 3). Authemayou et al. (2018) used these windgaps to establish that an initial parallel, north-flowing drainage was defeated by the rise of upslope-facing normal fault scarps across stream courses. This defeat led to a incremental, northward migration of the drainage divide. Several windgaps straddle the current divide between north-flowing and south-flowing streams, indicating that the northward migration of the drainage divide is still ongoing. Other windgaps (Fig. 4C) are not associated with normal faults. These are found along E-W-trending streams in the south-central part of the island near the Keradu Bay (Fig. 3), close to fish-hook tributaries (Fig. 4A). They reveal that, in this area, east-flowing rivers (Fig. 4B) were captured by southwestward- to southward-flowing coastal streams. Longitudinal profiles along the course of the former river valleys (Fig. 4D) reveal that the paleodrainage has been affected since its capture by southwestward tilting (Fig. 4C).

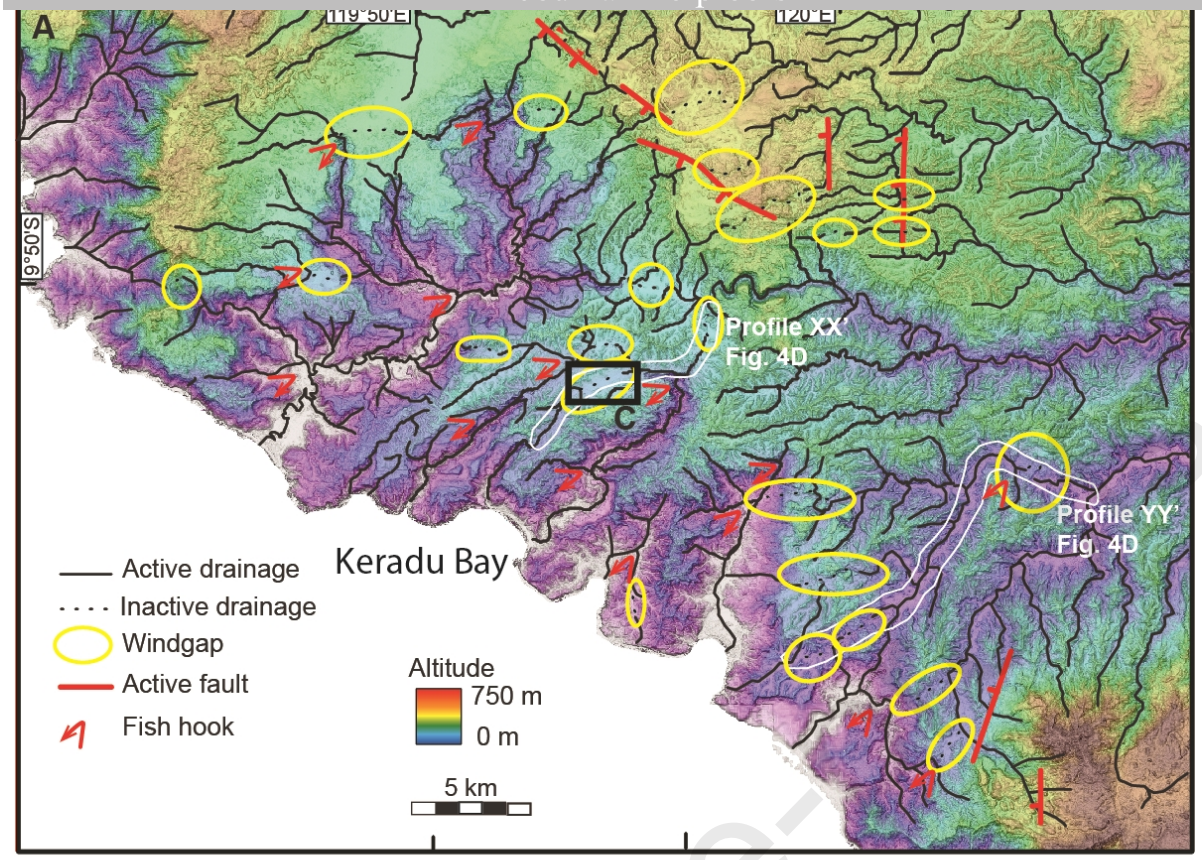
A
119°50'E
120°E
9°50'S
Profile XX'
Fig. 4D
C
Profile YY'
Fig. 4D
Keradu Bay
Active drainage
Inactive drainage
Windgap
Active fault
Fish hook
Altitude
750 m
0 m
5 km

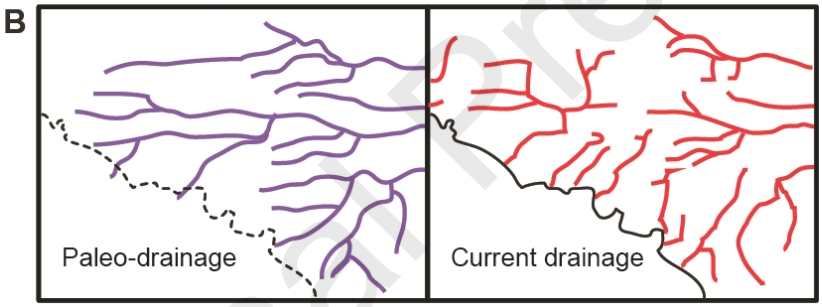
B
Paleo-drainage
Current drainage

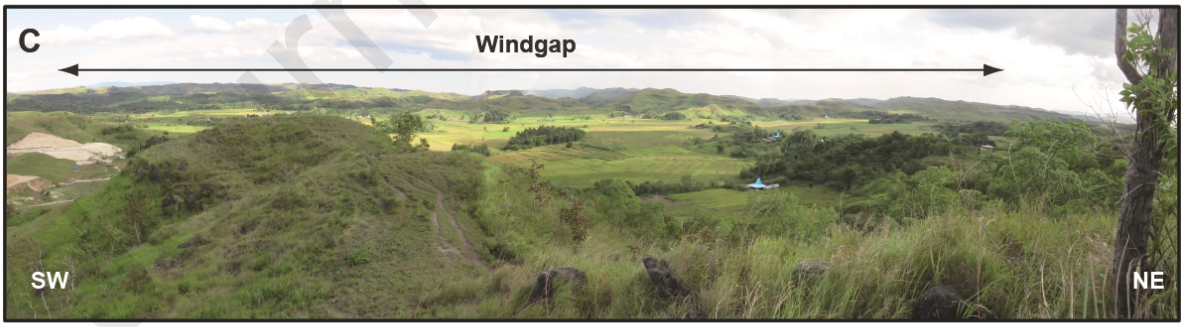
C
Windgap
SW
NE

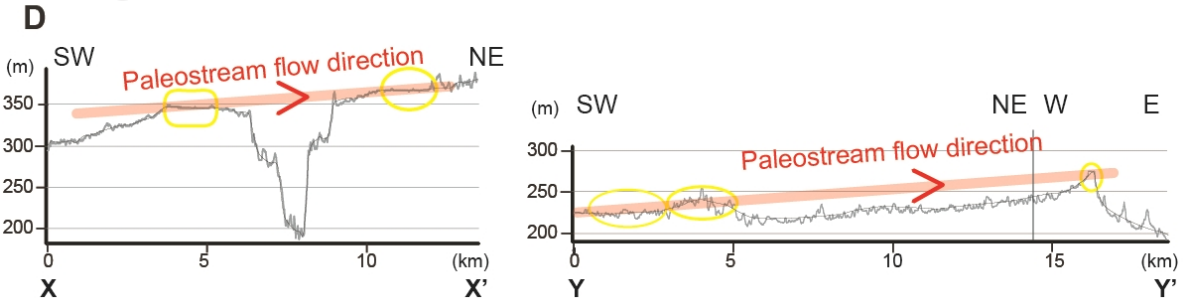
D
(m)
SW
Paleostream flow direction
NE
350
300
250
200
0
5
10
(km)
X
X'
(m)
SW
NE
W
E
Paleostream flow direction
300
250
200
0
5
10
15
(km)
Y
Y'

Figure 4: Windgaps and E-W trending streams in the south-central part of Sumba. (A) DEM showing the current drainage network and the location of windgaps and faults. (B) Comparison of the reconstructed drainage and the current drainage in the same area as figure 4A. (C) Field view of a large E-W-trending wingap. See location on figure 4A. (D) Topographic profiles along the floor of abandoned river valleys, evidencing back-tilting. Red lines represent former flow directions along these valleys. See location on figure 4A.

4.3. Topographic and coral reef terraces analyses

The accordance of regional hillslope and bedding over most of Sumba Island demonstrates that its relief is essentially structural (Authemayou et al., 2016). Low precipitation rates (300 $mm.yr^{-1}$), high infiltration rates in the carbonates, and the recent emergence of the island together best explain the low degree of dissection associated with the uplift. Therefore, the general relief of Sumba represents the integrated deformation of the island since its emergence during the Pliocene. Its coral reef terraces, by contrast, specifically record a more recent, Quaternary pattern of deformation.

The general shape of the island changes across the Kambarinu River (Fig. 5). West of the river, Sumba is dominated by the E-W trending, elongated and flat Waikabubak massif, which reaches a maximum elevation of ~900 m (Fig. 5B). East of the river, Sumba is dominated by the Kannanggar massif, which culminates at 1,225 m. The Kambarinu drainage catchment almost connects the northern coast to the south coast (Fig. 5A). The drainage catchment is associated with a change in the style of structural deformation on either side of the river (Fig. 5A). The topographic asymmetry is noticeable on the N-S-

trending swath profiles of the central and eastern parts of the Island (Figs. 5D, E). On the western part of the Island, the topography is symmetric, but afterretro-deformation of normal faulting, the topographic profile becomes asymmetrical (Fig. 5C).

Uplifted coral reef terraces are preserved along the northern, western and eastern coastlines. A prominent coral reef terrace, formed during MIS 11 at Cape Laundi (Pirazzoli et al., 1993), was mapped from Cape Karoso to Cape Undu by Nexer et al. (2015) (Fig. 5). Along-shore variations in the elevation of the MIS 11 coral reef terrace along the northern coast (black line, Fig. 5B) reveal a progressive eastward increase in uplift, from uniformly low values (10-20 m) between Cape Karoso (at the western end of the island) and the western boundary of Cape Sasar, to high values from Cape Sasar to Waingapu Bay (up to 220 m), followed by a decrease to Cape Undu (down to 130 m) (brown line, Fig. 5B). An homothetic pattern of uplift with a higher degree of tilting affects higher, more dissected coral reef terraces (blue and green lines, on Fig. 5F). It does not match, however, the uplift field documented by the overall asymmetric shape of Sumba Island. In western Sumba, northward tilting is evidenced along the western coast by the tilt of the coral reef terraces. The lower coral reef terrace also exhibits several discrete vertical offsets across E-W trending normal faults. The variations in the elevation of the coral reef terraces conform to the topography of the western island. (Fig. 5B).

Coral reef terraces located in the Western zone along a N-S transect are offset by down-to-the-south normal faulting and the upper terrace shows a northward tilting (Fig. 5C). Projections of terrace elevations in the central zone and in the eastern zone along NE-SW transects do not show clear evidence of a deformation pattern (Fig. 5D and Fig. 5E). But, a 100 km long N-S profile of terrace elevations from Cape Sasar to Cape Undu illustrates the deformation of the terrace sequence (Fig. 5F). The overlapping lines (terrace back-edge elevations) for the central zone and eastern zone transects illustrate the progressive change

in terrace elevation that occurs along the north coast of Sumba east of Cape Sasar (Fig. 5F). The progressive changes in elevation are consistent with folding and tilting of the terrace surfaces. Based on the elevation pattern, we infer the presence of a fold axis at the apex of the folded terrace sequence, located near Waingapu Bay, and a second near Cape Sasar (Figs. 5A and 5F).

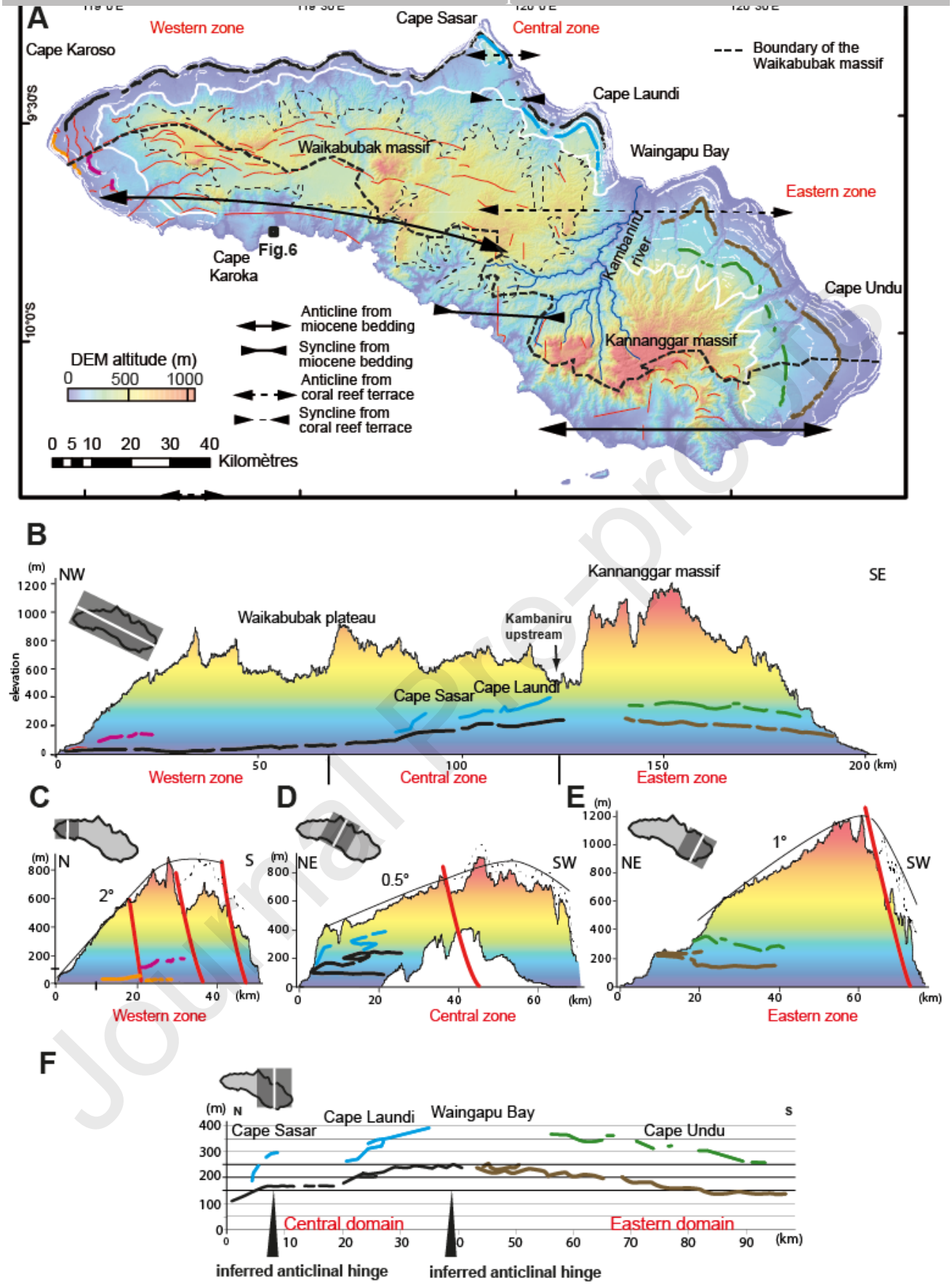

Figure 5: Distribution of coral reef terraces in map view and along cross sections,

compared to the topography of Sumba Island. (A) Spatial distribution of coral reef terraces around Sumba Island, projected onto the Tandem-X DEM. White broad line corresponds to the upper boundary of the coral reef terraces. White lines indicate inner edge of the major coral reef terraces. Green, brown, black, blue, pink, orange lines show the most continuous terraces. (B) Projection of coral reef terraces on a NW-SE-trending elevation swath profile. (C), (D), (E) Projection of coral reef terraces in the western zone, central and eastern zones on a N-S, NE-SW, NE-SW-trending elevation swath profiles, respectively. Black dotted lines and thin lines show the inferred topographic flexure with and without erosion and after retro-deformation of normal faulting, respectively. Slope values of the northern island flank are indicated on profiles. (F) North-south coral reef terrace elevation transect from the eastern side of Cape Sasar to Cape Undu.

Along the southern coast, we found previously undocumented coral reef terraces to the east of Cape Karoka (Figs. 5A and 6). Their presence implies that the south coast is also uplifting. At this location, near the village of Waiwuang, we surveyed an unmapped sequence of coral reef terraces, trackable up to an elevation of 250 m (site 1). The sequence includes 11 main coral reef terraces (Figs. 5A, 6A and 6B). Their extent is restricted to a paleo-embayment, on the eastern side of Cape Karoka. They may owe their preservation to their location in this bay, sheltered from the rapid coastal erosion that otherwise affects all the southern, windward coast of Sumba Island. The sequence is discontinuous and its remnants are found at various sites (site 1, site 2 and site 3). The DGPS profiles (Figs. 6B to 6D) reveal: 1st, that at site 1, the topmost terrace (250 ± 10 m a.s.l.) has a flat top hosting preserved coral heads (Fig. 6B); 2nd, that at site 2, the inner shorelines of the lowest terraces (T1, T2 and T3) stand at elevations of 4 ± 1 m, 22 ± 2 m, and 50 ± 2 m (Fig. 6C); and 3rd, that at site 3, the inner

shoreline angles of terraces (T5, T6, T7 and T8) stand at elevations of 102 ± 2 m, 125 ± 2 m, 153 ± 2 m and 166 ± 2 m. Terrace T1 contains beach sands (site 2, Fig. 6C). We dated a gastropod shell enclosed in these beach sands (sample 18.2, Fig. 6C, Table 1) using ^{14}C and U/Th dating yielded ages of 0.15 ka and 3.4 ka, respectively (Table 1). Despite the scarcity of recrystallization of aragonite to calcite, the shell may have undergone post-depositional diagenesis or detrital contamination (Szabo and Rosholt, 1969; Kaufman et al., 1971), which would account for the discrepancies between ^{14}C and U/Th dating. Regardless, these ages imply that terrace T1 formed during the Holocene.

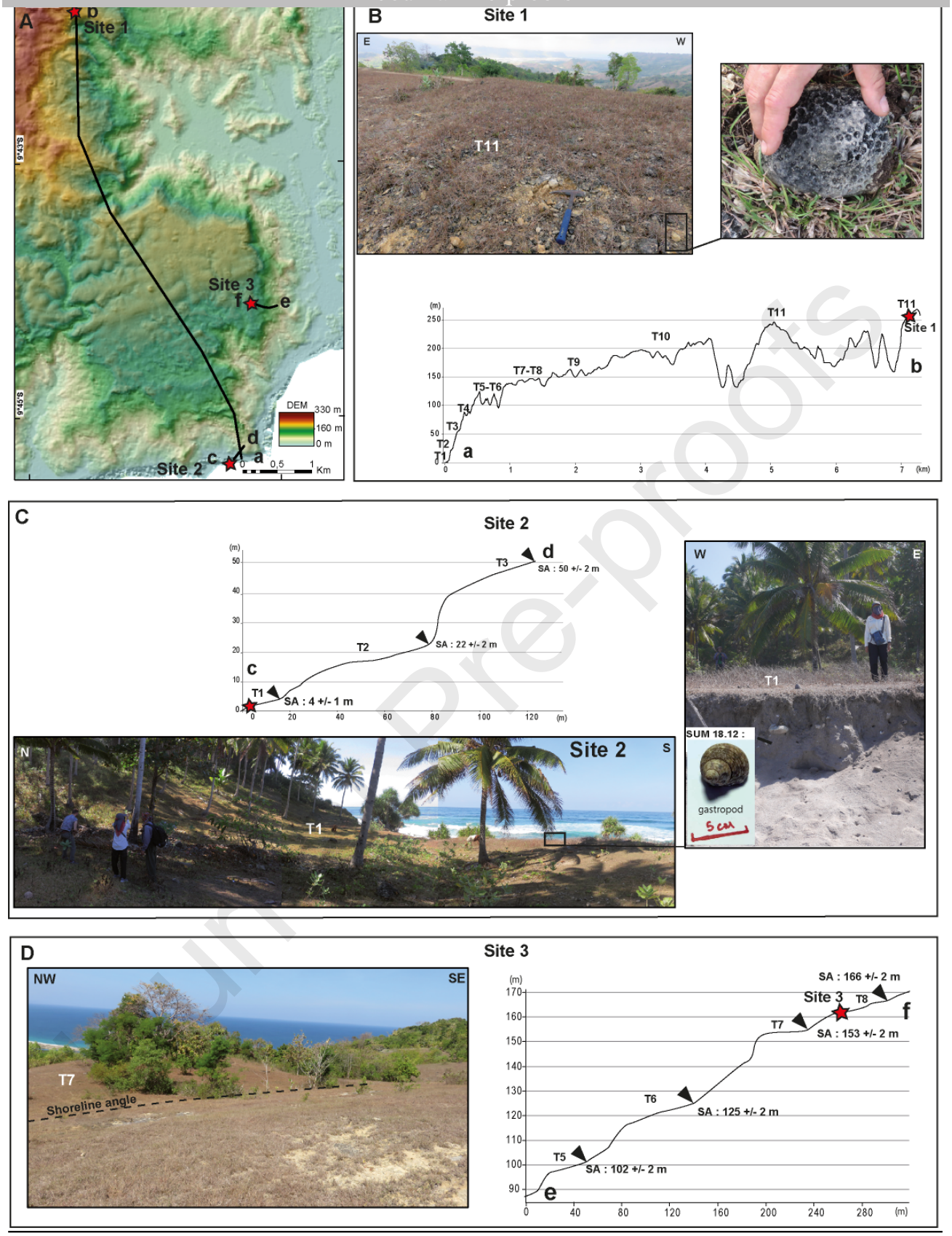

Figure 6: Sequences of coral reef terraces east of Cape Karoka. (A) Shaded DEM showing the location of the topographic profiles and field photographs displayed on

panels B, C, and D. (B) Site 1: field photographs and DGPS topographic profile showing coral reef terrace numbers and site location. (C) Site 2: topographic profile and field photographs of the lowermost terraces (T1, T2 and T3) south of the village of Waiwuang. (D) Site 3: topographic profile and field photographs of the intermediate terraces T5, T6, T7, and T8. Photograph shows inner shoreline angle of T7.

4.4. Focal mechanisms

The spatial distribution of shallow earthquake focal mechanisms (<50 km) highlights the styles of deformation occuring around Sumba island. To the southwest, along the trench axis, a cluster of focal mechanisms characterized by dominant normal motion (green beach balls, Figs 1B) and E-W trending nodal planes is interpreted to be related to the bending of the oceanic plate along the E-W-striking Java trench. Such focal mechanisms are absent east of 120E longitude, suggesting that the lower plate does not bend as vigorously into the trench to the east. The change in the pattern of earthquake occurrence coincides with the transition from oceanic crust to continental crust and a change in style of deformation, consistent with the introduction of higher-buoyancy continental crust into the subduction zone. North of Flores and Sumbawa islands, E-W oriented thrust faults (Flores thrust zone) are likely related to back-arc thrusting along the eastern Sunda arc (e.g. McCaffrey and Nabelek, 1984). South of the western part of the Sumba island, numerous events with reverse focal mechanism (purple balls on Figs. 1B and 7) reveal the presence of E-W oriented reverse faults or events on the interface. Farther east, some events with dominantly reverse focal mechanisms occur at the toe of the offshore slope, south of the central part of Sumba island. These events indicate that subduction shortens the fore-arc basin as well as the back arc domain on the Flores thrust. Rotations of the strike of reverse faults from E-W to NW-SE, south of Sumba, suggest that these offshore thrusts follow the sigmoidal shape

of the Sumba island. Scattered strike-slip focal mechanisms occur between the two clusters of reverse earthquakes, mainly west of Sumba island (red balls on Figs. 1B and 7) on N-S to NNW-SSE and E-W to ENE-WSW-striking faults. N-S to NNW-SSE-striking faults are inferred to accommodate dextral motion and appear associated with N-S to NNW-SSE discontinuities in the seafloor bathymetry (Fig. 7). The style of deformation and topographic discontinuities define a large-scale left restraining bend in a dextral shear couple above the transition zone between oceanic and continental subduction; referred to here as the West Sumba Shear Zone (WSSZ, Fig. 7). NNW-SSE fault segments extend approximately 100 km from the inflection in the trench axis northward (Fig. 7). They then bend westward (south of western Sumba) and extend another approximately 100 km toward Lombok Basin, and bend back to a NW direction along the series of dextral transpressional faults mapped by Luschen et al. (2011) (Fig. 7). The fold and thrust belt south of western Sumba and the folding of western Sumba Island may be the result of contraction across this broad left restraining bend.

Few focal mechanisms are found offshore, east of Sumba: two E-W trending thrusts and a single E-W normal solution (Figs 1B and 7). In the Savu basin (Fig. 1B), focal mechanisms are also rare; they show sinistral strike-slip deformation on the NE-SW planes in the southern and middle parts of the basin, and dextral motion along E-W plane north of the basin. Reverse focal mechanisms with EW oriented nodal planes appear in the northeastern corner of the Savu basin (Fig. 1B). They are related to the arc/continent collision localized in central Timor (Harris, 1991). Focal mechanisms with vertical and horizontal planes, mostly north of the Savu basin, could be produced by flat thrusting along the interplate subduction boundary or on a detachment level. Overall, the triangular Savu basin behaves as a rigid tectonic block only affected by modest transcurrent deformation. Along the Timor trough two focal mechanisms (strike-slip and reverse) indicate sinistral transpression along this

boundary (Fig. 1B). On the Australian margin, dextral strike-slip focal mechanisms have been recorded (Keep et al., 2012) .

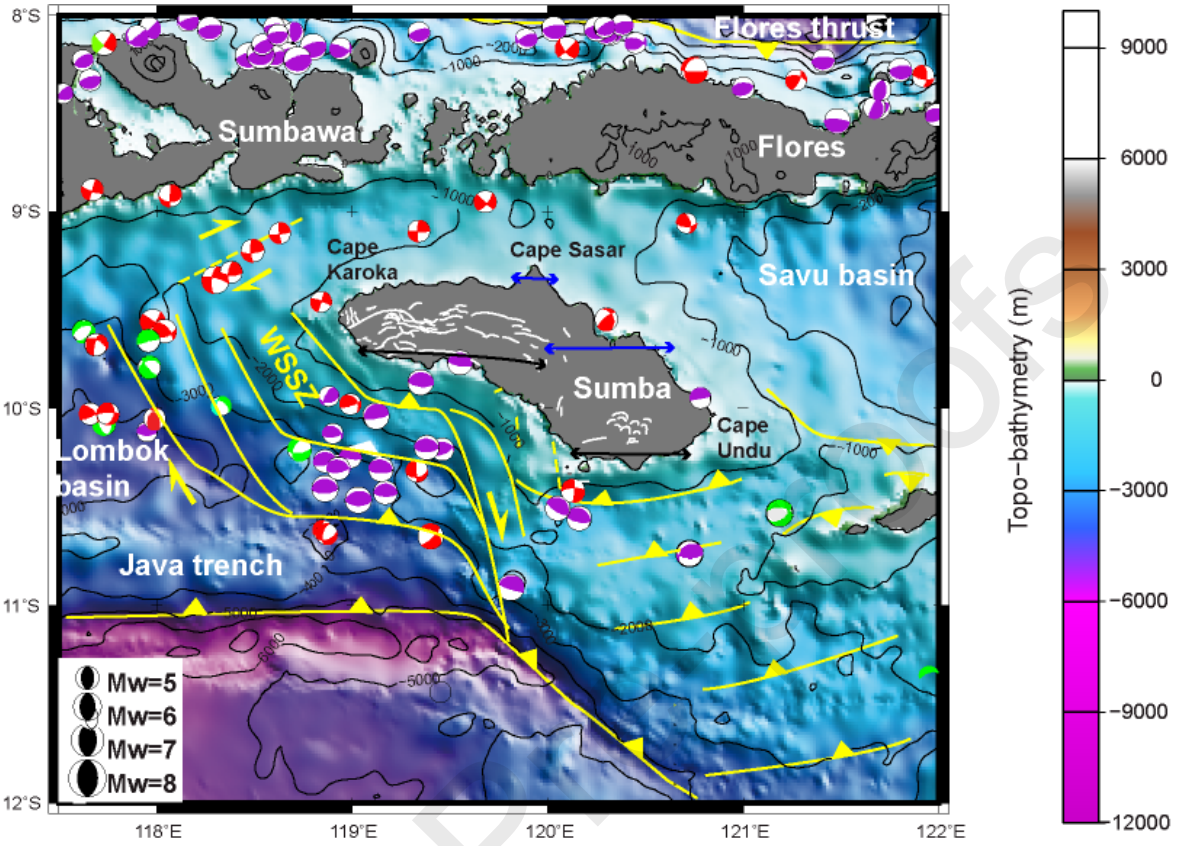

Figure 7: Structural map around Sumba island, and focal mechanisms of shallow (<50 km) earthquakes from GCMT solutions (www.globalcmt.org). Beachball size scales with earthquake magnitude; colors indicate kinematics (green: normal faulting, red: strike-slip faulting, purple: reverse faulting). White lines are one-shore faults revealed by the topographic and drainage analyses, yellow solid lines are faults mapped by Rigg and Hall (2011, 2012) and Lűschen et al. (2011) and our study, black lines with arrows show anticline axis deduced from orientations of Miocene strata and blue lines with arrows show anticline axis deduced from coral reef terrace deformation patterns. WSSZ, West Sumba Shear Zone.

5. Discussion

5.1. Geomorphic and deformational evolution of the Sumba Island

The attitude of Miocene beds and the aspect of structural slopes of Sumba (Figs. 2 and 5C, 5D, 5E) indicate that the western and the eastern parts of the island are folded by two broad E-W trending south-verging asymmetric anticlines with axis located near the southern coast. This fold vergence is consistent with the location of major offshore topographic escarpments south of Sumba Island, with reverse focal mechanisms likely produced by south-directed reverse faults (Fig. 7). The fold orientation is in agreement with contraction generated by 15° convergence and the E-W orientation of the plate boundary between the Sunda Block and the Australian plate.

The stream morphology reveals that the drainage has evolved since the emergence of the island by folding. The development of a first order, strongly asymmetrical drainage correlated with the asymmetric folds, accompanied the progressive emergence of the island during the Pliocene (Fig. 8A and B), but this drainage has since readjusted to adapt to the changes in deformation patterns. The drainage first rearranged in response to the growth of normal faults in Western Sumba, where windgaps are found over the footwalls of the E-W-trending normal faults (Authemayou et al., 2018; Fig. 3). In Eastern Sumba, more moderate diversions of the drainage divide is inferred to be due to the activation of short, cuspate normal faults associated to gravitational collapse within the Kannanggar massif (Figs. 3 and 8A). River diversions resulted in a northward migration of the drainage divide (Fig. 8A). This migration records the northward expansion of normal faulting, resulting from continuing

gravitational collapse of the southern flanks of the asymmetric folds (Authemayou et al., 2018).

Within the syncline between the two Pliocene anticlines, stream deflections occur in an area seemingly devoid of clear tectonic dislocations (Figs. 3, 4). While the drainage divide lies in this area very close to the southern coast, these deflections indicate a large east-flowing paleo-drainage and a former extension of this drainage at, or more probably beyond the southern coastline (Fig. 8A). Therefore, we infer the presence of a former drainage divide located near, or beyond the southern coast of the island. It implies that a large piece of the southern part of the Pliocene Sumba Island has been submerged. This beheaded east-flowing drainage flowed within the synclinal depression between the two anticlines (Figs 8A and 8B). In this zone, the southward bending of the some paleovalleys could result from the northward migration of the Eastern Sumba folding during the Quaternary (Figs. 4D, 8A and 8C).

The pattern of Quaternary deformation has been constrained using the uplifted coral reef terraces around the island. Terrace uplift along the west coast documents an unchanged pattern of deformation since Pliocene time with a maximum uplift on the south side of the island, as the morphology of Quaternary marine terraces mimics Pliocene deformation responsible for the asymmetric drainage and the overall shape of the western part of the island (Figs. 3 and 5C). Along the south coast, near Cape Karoka (Fig, 5A), a major coral reef sequence was observed. An uplift rate cannot be calculated at this site with the elevation and age of the Holocene terrace because the uncertainty on this value is too high due to the unknown value of the glacial isostatic adjustment in the area, which may be more or less preponderant on the low elevation of the Holocene terrace (4+/-2m). However, given that at Cape Laundi where the uplift rate is maximum on the island, the terrace sequence peaks at 470 m with an uplift rate of about 0.5 mm/yr (Chauveau et al., 2021), the presence of the

terrace sequence more than 250 m high on the south coast of Sumba indicates a non-negligible uplift rate.

By contrast, in Eastern Sumba, Quaternary uplift is greater in the north than in the south, which is opposite to the Pliocene pattern of uplift, responsible for the initial emergence of the island (Figs. 5E, 8A). The highest Quaternary marine terrace deposits on Sumba (470 m elevation) are located near Cape Sasar, on the north tip of the island. This requires either formation of a younger more active fold along the north coast, or a migration of the deformation field in Eastern Sumba (Fig. 8C). Some uplift is also recorded in coral reef terraces south of Cape Undu (Figs. 5E and 5F). Major submarine scarps, in close proximity to the southern coast of the Eastern Sumba, are inferred to be the result of south-verging reverse faults (Fig. 7). Farther offshore, folded and thrusted Pliocene formations have been identified on seismic cross-sections south of the island (Rigg and Hall, 2012). Collectively these deformations indicated that the southern part of Eastern Sumba continues to undergo basement uplift, and that its surface keeps rising in elevation despite the gravitational collapse of its southern flank.

The evolution of deformation on Sumba Island deduced from the geomorphological analysis highlights an enlargement of the shortening zone in Quaternary time in Eastern Sumba (Figs. 8B and 8C). Growth of the contractional deformation field is coeval to the arrival of Scott Plateau, a promontory of thinned Australian continental crust, into the Banda trench east of Sumba Island. The greater buoyancy of the continental crust results in a lower contribution of down-going slab pull to the stress regime, promoting stronger coupling across the subduction interface between the Australian and Eurasian plates, thereby promoting shortening within the overriding plate, and more contractional strain along the fore-arc (Hall and Smyth, 2008; Haig 2012; Tate et al., 2017, Miller et al., 2021).

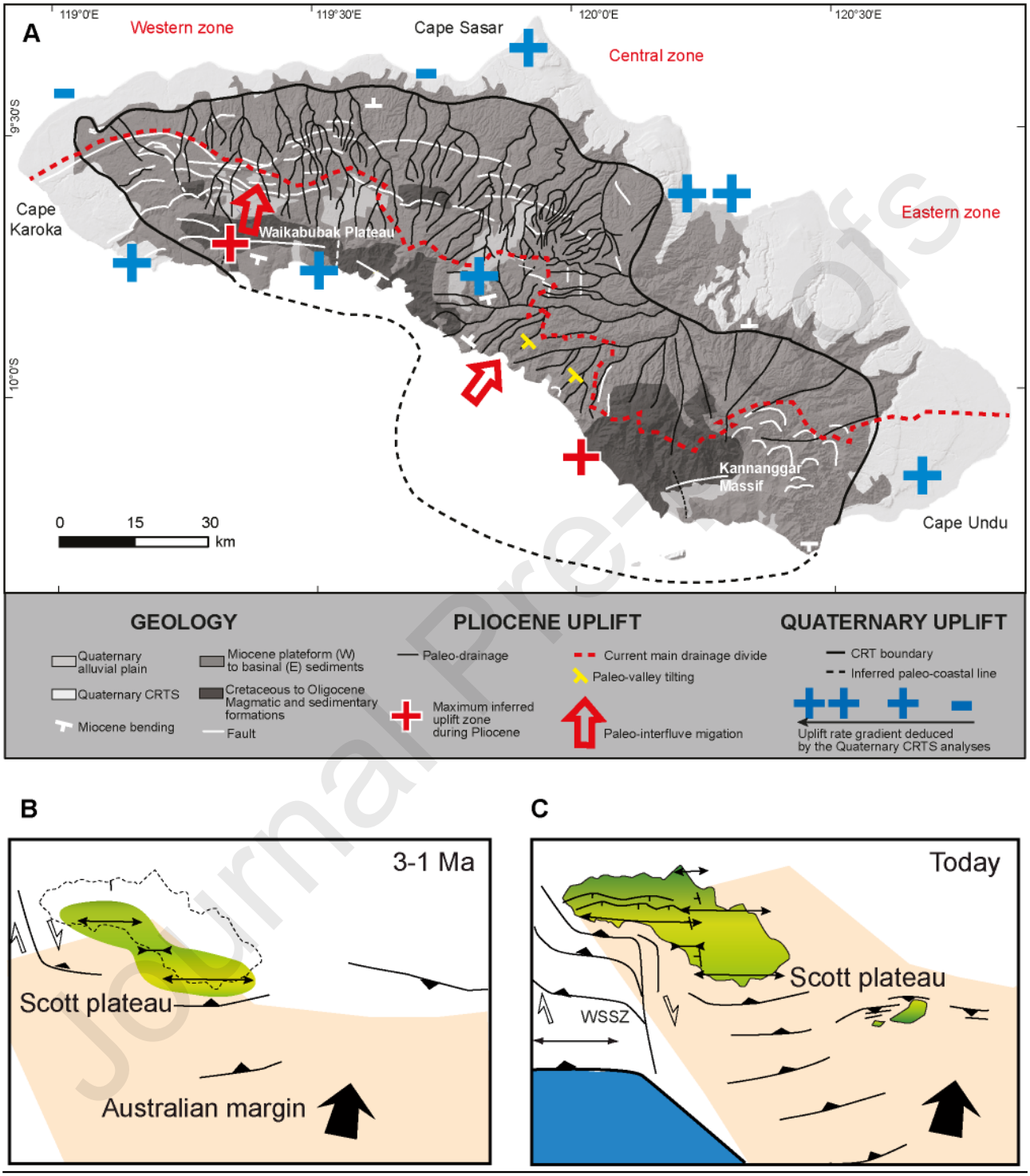

Figure 8: Morpho-tectonic evolution of Sumba Island. A- Temporal variation of uplift and drainage network in Sumba. B and C- Structural evolution of Sumba Island

since ~3 Ma.

5.2. Effects of the lateral transition from oceanic to continental subduction on the overriding plate

Fleury et al. (2009) proposed that deformation on Sumba Island results from the subduction of a topographic asperity on the Australian continental margin beneath the forearc region (Fig. 1D). If this were the case, however, the zone of maximal uplift, located above the asperity, would progressively drift northward as subduction of the asperity proceeds. We find instead that uplift on the Sumba Ridge broadens, rather than migrates. It is therefore better explained by more pervasive shortening in the overriding plate. However, more than a local asperity of the overriding plate, one can evoke a more global change of the nature of the crust with the subduction of a volcanic margin protrusion (Miller et al., 2021).

The Savu Rote accretionary prism, located south of Sumba, represents a significant broadening of the Sunda accretionary arc, from 130 km west of Sumba to 200 km, south of the island. This thickening results from greater retention of sediments within the accretionary prism, as continental crust gets subducted east of Sumba. The dextral transpressional shear zone (WSSZ, Figs. 7 and 8) that involves the western part of Sumba Island and generates a NNW-SSW trending positive flower structures (Luschen et al., 2011), lies next to a 150 km-long dextral offset of the subduction zone, from the Java trench to the Timor trough (Figs. 1B, 7 and 9). Luschen et al. (2011) consider that these wrench faults accommodate the differential shortening in the overriding plate, between the oceanic subduction in the west and the continental subduction/ incipient arc-continent collision in the east. The remarkable absence of normal focal mechanisms produced by the flexure of the down-going slab under

the thick prism is consistent with the rapidly changing nature of the down-going crust, as the buoyant Australian continental margin enters the trench (Fig. 1). Millet et al. (2021) consider that this change coincides with the edge of the volcanic margin protusion of the Australian continental margin.

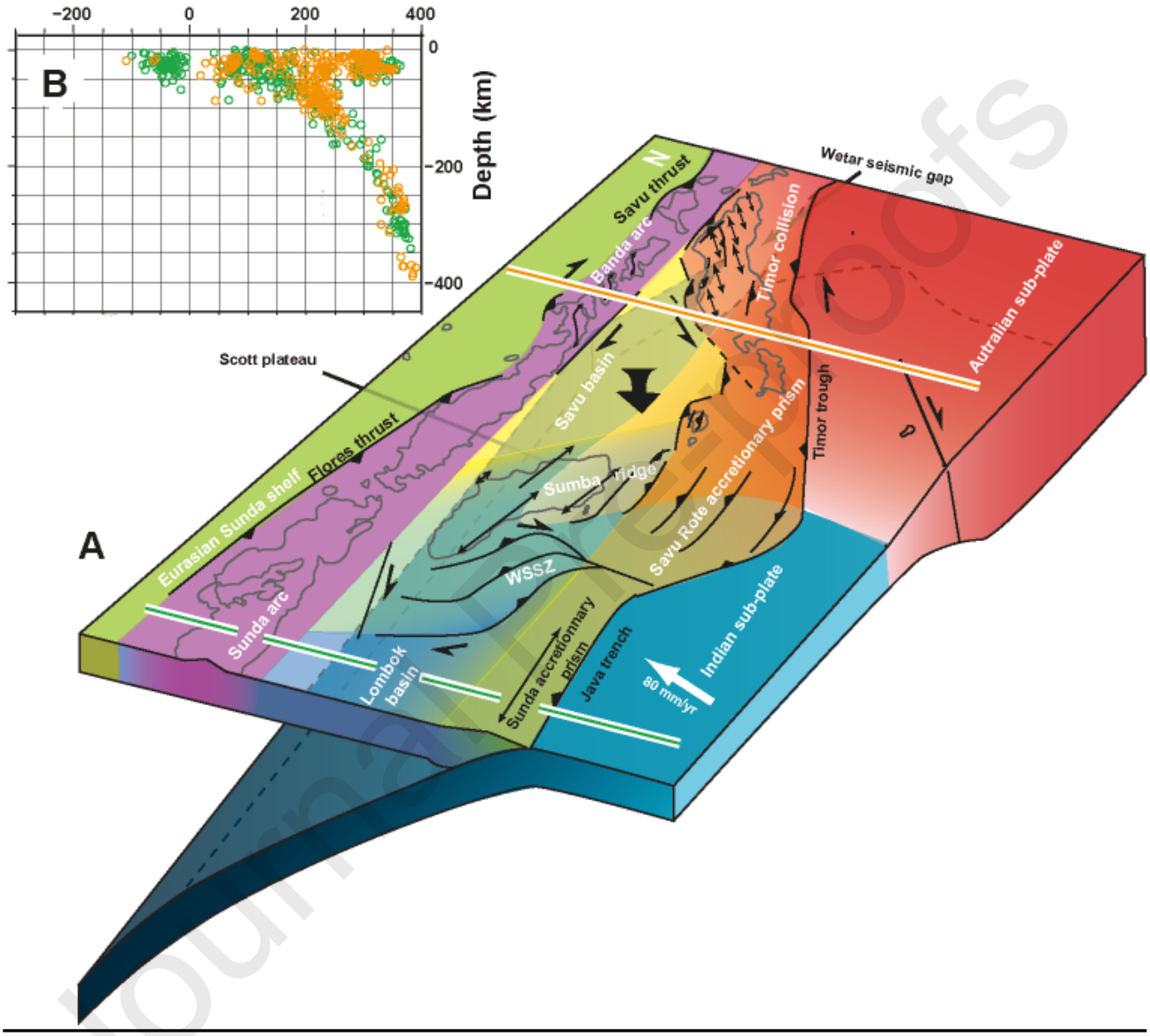

Figure 9: Geodynamic interpretation of the Lesser Sunda islands area. (A) 3D block diagram showing the lateral transition from oceanic to continental subduction, and associated fore-arc deformation. (B) Location of earthquake hypocenters along two transects across the subduction zone, under the Sumba Ridge (Submap, Heuret and Lallemand, 2005). Location of the green and orange transects on Fig. 9A.

Analogue and numerical experiments aimed at exploring deformation produced in the overriding plate at the oceanic-continental crust transition (Guillaume et al., 2013; Li et al., 2013; Duretz et al., 2014; Burov et al. 2014; Magni et al. 2014; 2017; Sternai et al. 2016) consistently indicate that the trench becomes increasingly deformed, as subduction stalls in front of the continent, while subduction proceeds by relative slab roll-back over the oceanic domain. As a result, the plate boundary is progressively offset at the ocean/continent transition, where a transcurrent regime may be established in both the downgoing slab and the overriding plate. In the area of study, such twisting of the slab across the oceanic/continental subduction remains poorly imaged by earthquake location data (Fig. 9B) and seismic tomography (Widiyantoro and van der Hilst, 1996; Hall and Spakman, 2015; Zenonos et al., 2019; Harris et al., 2020). The recent ingress of the continental crust into the trench (< 4Ma; Harris, 2011) may account for the absence of clear slab tear observed above the transition zone. Numerical modelling suggests that this process may require up to 15 Ma, at a contraction rate of 3 $cm.yr^{-1}$ for a tear to develop (Duretz et al., 2014). Even the compression rate in this study area is more than twice that used in the numerical modeling, which can halve the response time of slab tearing, the 4 Ma age of continental Australian margin subduction initiation is not sufficient to see any effect.

Besides, these rates have probably decreased following the arrival of the Australian continent into the trench, which has been documented along the Timor trough (Harris, 1991; Nugroho, 2009). The subducting leading edge of the Australian continental lithosphere (Scott Plateau) is continuing to migrate northward, but at a slower rate than the Indo-Australian oceanic crust beneath Lombok Basin. The leading edge of the subducted continental crust is beneath northern Sumba, in the area where the highest uplift rates were observed. The area from Cape Sasar to Cape Undu (Eastern Sumba) and south to the island

(on the east side of the WSSZ) is considered as a unique tectonic domain characterized by pervasive crustal shortening along a series of thrust faults above the marginal Australian continental crust (Figs. 8, 9). A second tectonic domain lies along the west side of continental crust, where the differential motion between the continental and oceanic elements of the subducting Indo-Australian plate is accommodated along the WSSZ. Deformation along the shear zone involves a combination of dextral and reverse faults that follow the continental margin. Because the oceanic domain is moving northward at a higher relative velocity compared to the part of the Australian continental domain underlying Sumba (Scott plateau) (Fig. 9), the inherited shape of the continental margin is controlling the shape of the deformation zone (Husson et al., 2021). Some of the strain is transmitted into the backstop resulting in the formation of the folds on Sumba Island, which are recorded through the drainage basin evolution and deformation of Quaternary marine strandlines on the Island.

To accommodate the increasing difference in subduction rate between the oceanic subduction in the west and the slowing continental subduction in the east, other structures are involved. In particular, the Australian passive margin has been reactivated into a 1,400km-long dextral shear zone (Hengesh and Whitney, 2016) (Fig. 9A). As this shear zone enters the trench, shear stress could be transferred, across the subduction interface, into the overriding plate, favored by the higher degree of interplate coupling occurring north of the Australian continent. Such transfer has been documented at the Kamchatka triple junction (Pedoja et al., 2013).

Spatial variations in forearc rheology and crustal thickness could also help focus deformation within Sumba Ridge. Indeed, the ridge is regarded as a 22-24 km-thick fragment of continental arc crust, flanked to the west by the 9-11 km-thick oceanic crust of the Lombok

basin (Hall and Smyth, 2008; Snidgin et al., 2009; Planert et al., 2010). The variations in crustal composition affecting the downgoing slab are therefore mirrored by similar variations in crustal thickness and nature within the overriding plate (Planert et al., 2010; Lüschen et al., 2011). Such configuration reinforces, 1st, lateral variations in interplate coupling, 2nd the fragmentation of the overriding plate into discrete tectonic blocks, and last, the concentration of dextral shear along lithological boundaries, and in particular at the boundary between the Lombok basin and the Sumba Ridge producing the West Sumba Shear Zone (Fig. 9).

The transcurrent structure bounding the west side of Sumba Ridge can be envisioned as a conjugate of the NE-SW left-lateral transpressional zone of western Timor Island (Charlton et al., 1991; Koulali et al., 2016; Nugroho et al., 2009; Figs. 1B and 9A). Right-lateral shear also occurs farther north within the Banda arc according to GPS data (Koulali et al., 2016), focal mechanisms (Fig. 14 in Lüschen et al., 2011), and en-échelon structures along the Lesser Sunda Islands (Muraoka et al., 2002). Convergence and incipient collision with the Australian continent therefore appears to be accommodated by pervasive shortening of the Australian continental margin in eastern Timor and by more localized wrenching on discrete transpressional zones farther west (Harris, 1991; Duffy et al., 2013). These later allow incipient southwestward lateral escape of the Savu-Sumba block (Fig. 9A), which had already been identified as a semi-rigid block by Nugroho et al. (2009), Koulali et al. (2016) and Hengesh and Whitney (2016). The extrusion of this block could explain the southward migration of the deformation front in the Savu Rote accretionary prism, and the apparent dextral offset of this deformation front west of the Sumba ridge. However, the bulge of the deformation front in the Savu Rote accretionary prism is also explained by a lowering in the taper angle due to lowering coefficient of friction along the basal decollement consisting of a 1000 m thick deposit of mostly smectite (Harris, 1991).

Conclusion

The deformation pattern across Sumba Island varies in time and space in a pattern consistent with the geodynamics of the Indian-Australian and Eurasian plate boundaries. During the Pliocene, the arrival of the Australian continental margin into the subduction zone produced folding in the fore-arc and the emergence of Sumba Island. On this island, maximum uplift of the southern part induced the gravitational collapse and dismantling of one third of the island. Remnants of the paleo-drainage of this paleo-relief are still present near the southern coast and attest of this evolution. During the Quaternary, folding propagated northward and eastward in eastern Sumba while the subduction of the Australian continental margin proceeded under the Eurasian plate. The numerous strandlines of coral reef terraces along the northern coast of the island result from the widening of the deformation zone and subsequent uplift. South of Sumba, we report a previously unmapped sequence of coral reef terraces of restricted lateral extension and offshore focal mechanisms with reverse motion, which together indicate that shortening and uplift are still ongoing all along the accretionary prism. The boundary between Sumba ridge and Lombok basin was reactivated in a dextral transpressive regime in order to accommodate the lateral variations of convergence rates along the plate boundaries from the Java trench to the Timor trough. We infer this boundary to be a several hundred km-long dextral transpressional shear zone with a large left restraining bend south of Sumba Island. The eastward decrease of subduction rate is caused by the longitudinally increasing interplate coupling. Meanwhile, the impingement of the Australian margin on Timor island may have triggered the southwestward extrusion of the Savu basin/Sumba ridge block, accommodated along the West Timor sinistral transpressive structure, the Banda arc dextral

transpressive zone and the Sumba ridge dextral transpressive zone. This block escape promoted the enlargement of the Rote-Savu accretionary prism south of Sumba amplifying the dextral offset of the Eurasian-Indian-Australian plate boundary. These displacements, however, were not accompanied by a southward displacement of the trench as predicted by lithospheric deformation models. The crustal deformation and heterogeneity of the Savu basin partially masks this behavior.

Acknowledgements

This work was supported by public funds received in the framework of GEOSUD, a project (ANR-10-EQPX-20 and ANR-10-LABX-19-01, Labex Mer, CLIMORESO, C. Authemayou) of the program "Investissements d'Avenir" managed by the French National Research Agency, the INSU Tellus Syter program (SECOMAS, C. Authemayou), the CNES TOSCA program (CETTROPICO, C. Authemayou). We thank the German Aerospace Center to provide us the TanDEM-X data for our study zone. We thank the State Ministry of Research and Technology of Indonesia “RISTEK” that allowed us to conduct the field trip to Sumba (research permit 680/FRP/E5/Dit.KI/IV/2017). We thank also the National Geographic Explorer grant (no CP 087R 17) to support the Indonesian researchers (Sri Yudawati Cahyarini, Vera Christanti Agusta, and Danny Hilman Natawidjaja). D. Scholz is thankful to the DFG for funding (SCHO 1274/11-1 and INST 247/889-1). Finally, we thank Hengesh, James, and a second anonymous reviewer for fruitful discussions on former versions of this manuscript.

References

Authemayou, C., Brocard, G., Delcaillau, B., Molliex, S., Pedoja, K., Husson, L., ... Cahyarini, S. Y. 2018. Unraveling the roles of asymmetric uplift, normal faulting and groundwater flow to drainage rearrangement in an emerging karstic landscape. *Earth Surface Processes and Landforms*, *43*(9), 1885-1898.

Abdullah, C. I., Rampnoux, J. P., Bellon, H., Maury, R. C., & Soeria-Atmadja, R. (2000). The evolution of Sumba Island (Indonesia) revisited in the light of new data on the geochronology and geochemistry of the magmatic rocks. Journal of Asian Earth Sciences, 18(5), 533-546.

Baillie, P., Keep, M., Duran, P.M., Carillo, E., Duval, G. 2019. Broadband seismic imaging around the Banda Arc : changes in the anatomy of offshore fold-and-thrust belts. From : Hammerstein, J. A., Di Cuia, R., Cottam, M. A., Zamora, G., Butler, R. W. H., (eds) folds and Thrust belts : Structural Style, Evolution and Exploration. Geological Society, London, Special Plublications, 490, http://doi.org/10.1144/SP490-2018-141.

Bard, E., Jouannic, C., Hamelin, B., Pirazzoli, P., Arnold, M., Faure, G., Sumosusastro, P. 1996. Pleistocene sea levels and tectonic uplift based on dating of corals from Sumba Island, Indonesia. *Geophysical Research Letters*, *23*(12), 1473-1476.

Bock, Y., Prawirodirdjo, L., Genrich, J. F., Stevens, C. W., McCaffrey, R., Subarya, C., Puntodewo, S. S. O., and Calais, E. (2003), Crustal motion in Indonesia from Global Positioning System measurements, *Geophysical Research Letters*, 108, 2367, doi:10.1029/2001JB000324, B8.

Boutelier, D., Oncken, O., Cruden, A. 2012. Fore-arc deformation at the transition between collision and subduction: Insights from 3-D thermomechanical laboratory experiments. *Tectonics*, *31*(2).

Burov, E., Francois, T., Yamato, P., Wolf, S. 2014. Mechanisms of continental subduction and exhumation of HP and UHP rocks. *Gondwana Research*, *25*(2), 464-493.

Charlton, T. R., Barber, A. J., Barkham, S. T. 1991. The structural evolution of the Timor collision complex, eastern Indonesia. *Journal of Structural Geology*, *13*(5), 489-500.

Chauveau, D., Authemayou, C., Pedoja, K., Molliex, S., Husson, L., Scholz, D., Godard, V., Pastier, A. –M., de Gelder, G., Cahyarini, Sri Y., Elliot, M., Weber, M., Benedetti, L., Jaud, M., Boissier, A., Christianti Agusta, V., Aribowo, S., Budd, A. F., Natawidjaja, D. H., ASTER Team. (2021). On the generation and degradation of emerged coral reef terrace sequences: First cosmogenic 36Cl analysis at Cape Laundi, Sumba Island (Indonesia). *Quaternary Science Reviews*, 269, 107144.

Duffy, B., Quigley, M., Harris, R., Ring, U. 2013. Arc-parallel extrusion of the Timor sector of the Banda arc-continent collision. *Tectonics*, *32*(3), 641-660.

Duretz, T., Gerya, T. V., Spakman, W. 2014. Slab detachment in laterally varying subduction zones: 3-D numerical modeling. *Geophysical Research Letters*, *41*(6), 1951-1956.

Fleury, J. M., Pubellier, M., de Urreiztieta, M. 2009. Structural expression of forearc crust uplift due to subducting asperity. *Lithos*, *113*(1-2), 318-330.

Fortuin, A. R., Roep, T. B., Sumosusastro, P. A., Van Weering, T. C., Van der Werff, W. 1992. Slumping and sliding in Miocene and Recent developing arc basins, onshore and offshore Sumba (Indonesia). *Marine Geology*, *108*(3-4), 345-363.

Fortuin, A. R., Roep, T. B., Sumosusastro, P. A. 1994. The Neogene sediments of Eastern Sumba, Indonesia—products of a lost arc?. *Journal of Southeast Asian Earth Sciences*, *9*(1-2), 67-79.

Fortuin, A. R., Van der Werff, W., Wensink, H. 1997. Neogene basin history and paleomagnetism of a rifted and inverted forearc region, on-and offshore Sumba, Eastern Indonesia. *Journal of Asian Earth Sciences*, *15*(1), 61-88.

Gibert, L., Scott, G.R., Scholz, D., Budsky, A., Ferrandez, C., Martin, R.A., Ribot, F., Leria, M. 2016. Chronology for the Cueva Victoria fossil site (SE Spain): Evidence for Early Pleistocene Afro-Iberian dispersals. *Journal of Human Evolution* 90, 183-197.

Guillaume, B., Husson, L., Funiciello, F., Faccenna, C. 2013. The dynamics of laterally variable subductions: laboratory models applied to the Hellenides. *Solid Earth*, *4*, 179-200.

Haig, D. W. 2012. Palaeobathymetric gradients across Timor during 5.7–3.3 Ma (latest Miocene–Pliocene) and implications for collision uplift. *Palaeogeography, Palaeoclimatology, Palaeoecology*, *331*, 50-59.

Hall, R. 2011. Australia–SE Asia collision: plate tectonics and crustal flow. *Geological Society, London, Special Publications*, *355*(1), 75-109.

Hall, R. 2012. Late Jurassic–Cenozoic reconstructions of the Indonesian region and the Indian Ocean. *Tectonophysics*, *570*, 1-41.

Hall, R., Spakman, W. 2015. Mantle structure and tectonic history of SE Asia. *Tectonophysics*, *658*, 14-45.

Hall, R., Smyth, H. R. 2008. Cenozoic arc processes in Indonesia: Identification of the key influences on the stratigraphic record in active volcanic arcs. *Formation and applications of the sedimentary record in arc collision zones*, *436*, 27.

Hamilton, W. B. (1979). Tectonics of the Indonesian region (Vol. 1078). US Government Printing Office.

Harris, R. A., 1991. Temporal distribution of strain in the active Banda orogen: a reconciliation of rival hypotheses, in Orogenesis in Action, (eds. E. Hall, G. Nichols, and C. Rangin), Spec V. Journal of Asian Earth Sci., V.6, No. 3/4, p. 373-386.

Harris, R. A., 1992. Peri-collisional extension and the formation of Oman-type ophiolites in the Brooks range and Banda arc, in: Ophiolites and Their Modern Oceanic Analogues, (ed. L. M. Parsons, B. J. Murton and P. Browning), Geol. Soc. of London, Spec. Pub. No. 60, p. 301-325.

Harris, R. 2011. The nature of the Banda Arc–continent collision in the Timor region. In *Arc-Continent Collision* (pp. 163-211). Springer, Berlin, Heidelberg.

Harris, R., Vorkink, M. W., Prasetyadi, C., Zobell, E., Roosmawati, N., Apthorpe, M. 2009. Transition from subduction to arc-continent collision: Geologic and neotectonic evolution of Savu Island, Indonesia. *Geosphere*, *5*(3), 152-171.

Harris, C. W., Miller, M. S., Supendi, P., Widiyantoro, S. 2020. Subducted Lithospheric Boundary Tomographically Imaged beneath Arc-Continent Collision in Eastern Indonesia. *Journal of Geophysical Research: Solid Earth*, *125*(8), e2019JB018854.

Hengesh, J. V., Whitney, B. B. 2016. Transcurrent reactivation of Australia's western passive margin: An example of intraplate deformation from the central Indo-Australian plate. *Tectonics*, *35*(5), 1066-1089.

Husson, L., Riel, N., Aribowo, S., Authemayou, C., de Gelder, G., Kaus, B. J. P, Mallard, C., Natawidjaja, D. H., Pedoja, K., Sarr, A. C., 2022. Slow Geodynamics and Fast Morphotectonic in the far East Tethys. *Geochemistry, Geophysics, Geosystems*, 23, e2021GC010167.

Kaufman, A., Broecker, W., Ku, T.-L. Thurber, D. 1971. The status of U-series methods of mollusk dating. *Geochimica et Cosmochimica Acta* 35, 1155-1183.

Keep, M., Hengesh, J., & Whitney, B., 2012. Natural seismicity and tectonic geomorphology reveal regional transpressive strain in northwestern Australia. Australian *Journal of Earth Sciences, 59*(3), 341-354.

Kopp, H. 2011. The Java convergent margin: structure, seismogenesis and subduction processes. *Geological Society, London, Special Publications*, *355*(1), 111-137.

Koulali, A., Susilo, S., McClusky, S., Meilano, I., Cummins, P., Tregoning, P., Syafi'i, M. A. 2016. Crustal strain partitioning and the associated earthquake hazard in the eastern Sunda-Banda arc. *Geophysical Research Letters*, *43*(5), 1943-1949.

Li, Z. H., Xu, Z., Gerya, T., Burg, J. P. 2013. Collision of continental corner from 3-D numerical modeling. *Earth and Planetary Science Letters*, *380*, 98-111.

Lüschen, E., Müller, C., Kopp, H., Engels, M., Lutz, R., Planert, L., Djajadihardja, Y. S. 2011. Structure, evolution and tectonic activity of the eastern Sunda forearc, Indonesia, from marine seismic investigations. *Tectonophysics*, *508*(1-4), 6-21.

Magni, V., Faccenna, C., van Hunen, J., Funiciello, F. 2014. How collision triggers backarc extension: Insight into Mediterranean style of extension from 3-D numerical models. *Geology*, *42*(6), 511-514.

Magni, V., Allen, M. B., van Hunen, J., Bouilhol, P. 2017. Continental underplating after slab break-off. *Earth and Planetary Science Letters*, *474*, 59-67.

McCaffrey, R., Nabelek, J. 1984. The geometry of back arc thrusting along the eastern Sunda arc, Indonesia: Constraints from earthquake and gravity data. *Journal of Geophysical Research: Solid Earth*, *89*(B7), 6171-6179.

Middleton, L.T., Porter, M.L., Kimmel, P.G., 1985, Depositional settings of the Chalk Hills and Glenns Ferry Formations west of Bruneau, Idaho, in Flores, R.M., and Kaplan, S.S., eds., Cenozoic paleogeography of west-central United States: Denver, Rocky Mountain Section, Society of Economic Paleontologists and Mineralogists, p. 37–54.

Miller, M. S., Zhang, P., Dahlquist, M. P., West, A. J., Becker, T. W., Harris, C. W. 2021. Inherited lithospheric structures control arc-continent collisional heterogeneity. *Geology*. *49* (6), 652-656.

Moresi, L., Betts, P. G., Miller, M. S., Cayley, R. A. 2014. Dynamics of continental accretion. *Nature*, *508*(7495), 245-248.

Muraoka, H. 2002. Tectonic. volcanic and stratigraphic geology of the Bajawa geothermal field, central Flores, Indonesia. *Bull. Geol. Surv. Japan*, *53*, 109-138.

Murray-Wallace, C. V., Woodroffe, C. D. 2014. Quaternary sea-level changes: a global perspective. Cambridge University Press. 484 pp.

Nexer, M., Authemayou, C., Schildgen, T., Hantoro, W. S., Molliex, S., Delcaillau, B., Regard, V. 2015. Evaluation of morphometric proxies for uplift on sequences of coral reef terraces: A case study from Sumba Island (Indonesia). *Geomorphology*, *241*, 145-159.

Nugroho, H., Harris, R., Lestariya, A. W., Maruf, B. 2009. Plate boundary reorganization in the active Banda Arc–continent collision: Insights from new GPS measurements. *Tectonophysics*, *479*(1-2), 52-65.

Obert, J.C., Scholz, D., Felis, T., Brocas, W.M., Jochum, K.P., Andreae, M.O. 2016 ^{230}Th/U dating of Last Interglacial brain corals from Bonaire (southern Caribbean) using bulk and theca wall material. *Geochimica et Cosmochimica Acta* 178, 20-40.

Pacheco, J. F., Sykes, L. R., Scholz, C. H. 1993. Nature of seismic coupling along simple plate boundaries of the subduction type. *Journal of Geophysical Research: Solid Earth*, *98*(B8), 14133-14159.

Pedoja, K., Authemayou, C., Pinegina, T., Bourgeois, J., Nexer, M., Delcaillau, B., Regard, V. 2013. “Arc-continent collision” of the Aleutian-Komandorsky arc into Kamchatka: Insight into Quaternary tectonic segmentation through Pleistocene marine terraces and morphometric analysis of fluvial drainage. *Tectonics*, *32*(4), 827-842.

Pirazzoli, P. A., Radtke, U., Hantoro, W. S., Jouannic, C., Hoang, C. T., Causse, C., Best, M. B. 1991. Quaternary raised coral-reef terraces on Sumba Island, Indonesia. *Science*, *252*(5014), 1834-1836.

Pirazzoli, P. A., Radtke, U., Hantoro, W. S., Jouannic, C., Hoang, C. T., Causse, C., Best, M. B. 1993. A one million-year-long sequence of marine terraces on Sumba Island, Indonesia. *Marine Geology*, *109*(3-4), 221-236.

Planert, L., Kopp, H., Lueschen, E., Mueller, C., Flueh, E. R., Shulgin, A., Krabbenhöft, A. 2010. Lower plate structure and upper plate deformational segmentation at the Sunda-Banda arc transition, Indonesia. *Journal of Geophysical Research: Solid Earth*, *115*(B8).

Rangin, C., Jolivet, L., & Pubellier, M. A. N. U. E. L. (1990). A simple model for the tectonic evolution of southeast Asia and Indonesia region for the past 43 my. *Bulletin de la Société géologique de France*, *6*(6), 889-905.

Rigg, J. W., Hall, R. 2011. Structural and stratigraphic evolution of the Savu Basin, Indonesia. *Geological Society, London, Special Publications*, *355*(1), 225-240.

Roep, T. B., Fortuin, A. R. 1996. A submarine slide scar and channel filled with slide blocks and megarippled Globigerina sands of possible contourite origin from the Pliocene of Sumba, Indonesia. *Sedimentary Geology*, *103*(1-2), 145-160.

Roosmawati, N., Harris, R. 2009. Surface uplift history of the incipient Banda arc-continent collision: Geology and synorogenic foraminifera of Rote and Savu Islands, Indonesia. *Tectonophysics*, *479*(1-2), 95-110.

Royden, L. H., Husson, L. 2009. Subduction with variations in slab buoyancy: models and application to the Banda and Apennine systems. In *Subduction zone geodynamics* (pp. 35-45). Springer, Berlin, Heidelberg.

Rutherford , E., Burke, K., Lytwyn, J. 2001. Tectonic history of Sumba Island, Indonesia, since the Late Cretaceous and its rapid escape into the forearc in the Miocene. *Journal of Asian Earth Sciences*, *19*(4), 453-479.

Satyana, A. H., Purwaningsih, M. E. 2011. Sumba area: Detached Sundaland terrane and petroleum implications. Proceedings Indonesian Petroleum Association, 35th Annual Convention, IPA11-G-009 (2011), pp. 1-32

Shulgin, A., Kopp, H., Mueller, C., Lueschen, E., Planert, L., Engels, M., Djajadihardja, Y. 2009. Sunda-Banda arc transition: Incipient continent-island arc collision (northwest Australia). *Geophysical Research Letters*, *36*(10).

Simons, W. J. F., Socquet, A., Vigny, C., Ambrosius, B. A. C., Haji Abu, S., Promthong, C., Spakman, W. 2007. A decade of GPS in Southeast Asia: Resolving Sundaland motion and boundaries. *Journal of Geophysical Research: Solid Earth*, *112*(B6).

Spakman, W., Hall, R. 2010. Surface deformation and slab–mantle interaction during Banda arc subduction rollback. *Nature Geoscience*, *3*(8), 562-566.

Sternai, P., Avouac, J. P., Jolivet, L., Faccenna, C., Gerya, T., Becker, T. W., Menant, A. 2016. On the influence of the asthenospheric flow on the tectonics and topography at a

collision-subduction transition zones: Comparison with the eastern Tibetan margin. *Journal of Geodynamics*, *100*, 184-197.

Szabo, B., Rosholt, J. 1969. Uranium-series dating of Pleistocene molluscan shells from southern California—An open system model. *Journal of Geophysical Research* 74, 3253-3260.

Tate, G. W., McQuarrie, N., Tiranda, H., van Hinsbergen, D. J., Harris, R., Zachariasse, W. J., Willett, S. D. 2017. Reconciling regional continuity with local variability in structure, uplift and exhumation of the Timor orogen. *Gondwana Research*, *49*, 364-386.

Thompson, W. G., Goldstein, S. L. 2005. Open-system coral ages reveal persistent suborbital sea-level cycles. *Science*, *308*(5720), 401-404.

Van der Werff, W., Prasetyo, H., Kusnida, D.,Van Weering, T. C. E. 1994. Seismic stratigraphy and Cenozoic evolution of the Lombok forearc basin, eastern Sunda Arc. *Marine geology*, *117*(1-4), 119-134.

Von der Borch, C. C., Grady, A. E., Hardjoprawiro, S., Prasetyo, H., Hadiwisastra, S. 1983. Mesozoic and late Tertiary submarine fan sequences and their tectonic significance, Sumba, Indonesia. *Sedimentary Geology*, *37*(1-2), 113-132.

Wensink, H., van Bergen, M. J. 1995. The tectonic emplacement of Sumba in the Sunda-Banda Arc: paleomagnetic and geochemical evidence from the early Miocene Jawila volcanics. *Tectonophysics*, *250*(1-3), 15-30.

Widiyantoro, S., van der Hilst, R. 1996. Structure and evolution of lithospheric slab beneath the Sunda arc, Indonesia. *Science*, *271*(5255), 1566-1570.

Yang, Q., Scholz, D., Jochum, K.P., Hoffmann, D.L., Stoll, B., Weis, U., Schwager, B., Andreae, M.O. 2015 Lead isotope variability in speleothems - A promising new proxy for hydrological change? First results from a stalagmite from western Germany. *Chemical Geology* 396, 143-151.

Zenonos, A., De Siena, L., Widiyantoro, S., Rawlinson, N. 2019. P and S wave travel time tomography of the SE Asia-Australia collision zone. *Physics of the Earth and Planetary Interiors*, *293*, 106267.

Table caption :

Table 1: ^{14}C dating and U/Th dating of sample 18.2 (119°26'38.88''E, 9°45'14.46"S).

Figure captions :

Figure 1: Geodynamic settings of Indonesia (A) and Sumba Island (B), modified from Rigg and Hall (2011; 2012) and Lűschen et al (2011).. Focal mechanisms of shallow earthquakes (<50km) from GCMT solutions (http://globalcmt.org; Dziewonski et al., 1981; Ekström et al.,

2012). Colors indicate focal mechanism (green: normal faulting, red: strike-slip faulting, purple: reverse faulting). C) NS-striking c section across the Sumba Ridge, east of Sumba Island, modified from Shulgin et al. (2009). (D) NS-striking geological section across Sumba Island, modified from Fleury et al. (2009).

Figure 2: Geology and tectonics of Sumba Island. (A) Shaded relief with main geological units, faults, and drainage lines. Fold axes are deduced from the structural measurements. (B) Photographs illustrating spatial variations in the dip of Miocene formations throughout the island (a, c, b, d, e, f). See Fig. 2A for location.

Figure 3: Geomorphologic map of the drainage pattern and tectonics features.

Figure 4: Windgaps and E-W trending streams in the south-central part of Sumba. (A) DEM showing the current drainage network and the location of windgaps and faults. (B) Comparaison of the reconstructed drainage and of the current drainage in the same area as figure 4A. (C) Field view of a E-W-trending large wingap. See location on figure 4A. (D) Topographic profiles along the floor of abandoned river valleys, evidencing back-tilting. Red lines represent former flow directions along these valleys. See location on figure 4A.

Figure 5: Distribution of coral reef terraces in map view and along cross sections, compared to the topography of Sumba Island. (A) Spatial distribution of coral reef terraces around Sumba Island, projected onto the Tandem-X DEM. White broad line corresponds to the upper boundary of the coral reef terraces. White lines indicate inner edge of the major coral reef terraces. Green, brown, black, blue, pink, orange lines show the most continuous terraces. (B) Projection of coral reef terraces on a NW-SE-trending elevation swath profile.

(C), (D), (E) Projection of coral reef terraces in the western zone, central and eastern zones on a N-S, NE-SW, NE-SW-trending elevation swath profiles, respectively. . Black dotted lines and thin lines show the inferred topographic flexure with and without erosion and after retro-deformation of normal faulting, respectively. Slope values of the northern island flank are indicated on profiles. (F) North-south coral reef terrace elevation transect from the eastern side of Cape Sasar to Cape Undu.

Figure 6: Sequences of coral reef terraces east of Cape Karoka. (A) Shaded DEM showing the location of the topographic profiles and field photographs displayed on panels B, C, and D. (B) Site 1: field photographs and DGPS topographic profile showing coral reef terrace numbers and site location. (C) Site 2: topographic profile and field photographs of the lowermost terraces (T1, T2, T3) south of the village of Waiwuang. (D) Site 3: topographic profile and field photographs of the intermediate terraces T5, T6, T7, and T8. Photograph shows inner shoreline angle of T7.

Figure 7: Structural map around Sumba island, and focal mechanisms of shallow (<50 km) earthquakes from GCMT solutions (www.globalcmt.org). Beachball size scales with earthquake magnitude; colors indicate kinematics (green: normal faulting, red: strike-slip faulting, purple: reverse faulting). White lines are one-shore faults revealed by the topographic and drainage analyses, yellow solid lines are faults mapped by Rigg and Hall (2011, 2012) and Lűschen et al. (2011) and our study, black lines with arrows show anticline axis deduced from orientations of Miocene strata and blue lines with arrows show anticline axis deduced from coral reef terrace deformation pattern. WSSZ, West Sumba Shear Zone.

Figure 8: Morpho-tectonic evolution of Sumba Island. A- Temporal variation of uplift and drainage network in Sumba. B and C- Structural evolution of Sumba Island since ~3 Ma.

Figure 9: Geodynamic interpretation of the Lesser Sunda islands area. (A) 3D block diagram showing the lateral transition from oceanic to continental subduction, and associated fore-arc deformation. (B) Location of earthquake hypocenters along two transects across the subduction zone, under the Sumba Ridge (Submap, Heuret and Lallemand, 2005). Location of the green and orange transects on Figure 9A.

CREDIT AUTHOR STATEMENT JAESSD2100572

Christine Authemayou : supervision, conceptualization, methodology, software, investigation, writing Original Draft, visualization, data curation, funding acquisition

Kevin Pedoja : validation, reviewing and editing

Denovan Chauveau : validation, reviewing and editing

Laurent Husson: validation, reviewing and editing

Gilles Brocard: data curation, validation, reviewing and editing

Bernard Delcaillau : validation, reviewing and editing

Julie Perrot : data curation, validation, reviewing and editing

Sonny Aribowo : data curation, validation

Sri Yudawati Cahyarini : data curation, validation

Mary Elliot : data curation, validation

Danny Hilman Natawidjaja : data curation, validation

Denis Scholz : data curation, validation

Author Agreement Statement

We the undersigned declare that this manuscript is original, has not been published before and is not currently being considered for publication elsewhere. We confirm that the manuscript has been read and approved by all named authors and that there are no other persons who satisfied the criteria for authorship but are not listed. We further confirm that the order of authors listed in the manuscript has been approved by all of us.We understand that the Corresponding Author is the sole contact for the Editorial process. She is responsible for communicating with the other authors about progress, submissions of revisions and final approval of proofsSigned by all authors.

Christine authemayou

Declaration of interest :

The authors of the manuscript entitled " "**Deformation and uplift at the transition from oceanic to continental subduction, Sumba Island, Indonesia.**" declare no competing interest.

Christine authemayou

^{14}C dating

mg C	Delta C13	pMC	Err pMC	Age BP	Err âge BP
1.15	0.50	93.18719	0.20274	145	145

U/Th dating

Calcite (%)	Aragonite (%)	238U [µg/g]	232Th [ng/g]	(234U/238U)	(230Th/238U)	age uncorrected [ka]	age corrected [ka]	(234U/238U)initial
< 1	> 99	0,0253	0,979	1,0989	0,0337	4,42	3,40	1,0998
		±	±	±	±	±	±	±
		0,0001	0,005	0,0024	0,0051	0,13	0,52	0,0025

Table 1

Click here to access/download;Table;table1.docx

^{14}C dating

mg C	Delta C13	pMC	Err pMC	Age BP	Err âge BP
1.15	0.50	93.18719	0.20274	145	145

U/Th dating

Calcite (%)	Aragonite (%)	238U [µg/g]	232Th [ng/g]	(234U/238U)	(230Th/238U)	age uncorrected [ka]	age corrected [ka]	(234U/238U)initial
< 1	> 99	0,0253	0,979	1,0989	0,0337	4,42	3,40	1,0998
		±	±	±	±	±	±	±
		0,0001	0,005	0,0024	0,0051	0,13	0,52	0,0025